

# Navigating Demand Uncertainty in Container Shipping: Deep Reinforcement Learning for Enabling Adaptive and Feasible Master Stowage Planning\*

Jaike van Twiller<sup>1</sup>, Yossiri Adulyasak<sup>2</sup>, Erick Delage<sup>2</sup>, Djordje Grbic<sup>1</sup>, Rune Møller Jensen<sup>1</sup>

<sup>1</sup> IT University of Copenhagen, Denmark

<sup>2</sup> HEC Montréal, Canada

{jaiv, djgr, rmj}@itu.dk,

{yossiri.adulyasak, erick.delage}@hec.ca

## Abstract

Reinforcement learning (RL) has shown promise in solving various combinatorial optimization problems. However, conventional RL faces challenges when dealing with real-world constraints, especially when action space feasibility is explicit and dependent on the corresponding state or trajectory. In this work, we focus on using RL in container shipping, often considered the cornerstone of global trade, by dealing with the critical challenge of master stowage planning. The main objective is to maximize cargo revenue and minimize operational costs while navigating demand uncertainty and various complex operational constraints, namely vessel capacity and stability, which must be dynamically updated along the vessel's voyage. To address this problem, we implement a deep reinforcement learning framework with feasibility projection to solve the master stowage planning problem (MPP) under demand uncertainty. The experimental results show that our architecture efficiently finds adaptive, feasible solutions for this multi-stage stochastic optimization problem, outperforming traditional mixed-integer programming and RL with feasibility regularization. Our AI-driven decision-support policy enables adaptive and feasible planning under uncertainty, optimizing operational efficiency and capacity utilization while contributing to sustainable and resilient global supply chains.

remains to address lesser-known yet critical planning challenges in supply chains. By addressing these challenges, we bridge the gap between theory and practice, enhancing the reliability and efficiency of worldwide supply chain operations.

Container shipping is a key component of the global supply chain, responsible for transporting 45% of annual goods valued at \$8.1 trillion [UNCTAD, 2021]. Due to its scale, it is often regarded as the cornerstone of worldwide trade and modern consumerism. However, this scale also has a significant environmental impact, with yearly CO2 emissions exceeding 200 million tonnes [Lloyd's List, 2022]. Despite this, container vessels are considered an environmentally friendly mode of transportation, due to their relatively low emissions per cargo ton-mile [Jensen *et al.*, 2018]. Consequently, container shipping is recognized to play a crucial role in the global green transition [European Commission, 2023]. Within container shipping, there are several interdependent and complex planning tasks, such as berth allocation [Martin-Iradi *et al.*, 2022], pre-marshalling [Hottung *et al.*, 2020], quay crane scheduling [Herup *et al.*, 2022], and container vessel stowage planning [Van Twiller *et al.*, 2024b]. Due to decision-making under demand uncertainty and various combinatorial aspects - such as capacity limits, seaworthiness requirements, minimizing overstocking and maximizing revenue - stowage planning is particularly challenging. To mitigate this challenge, stowage planning is often decomposed into the master planning problem (MPP), which involves the assignment of cargo to clusters of slots, and the slot planning problem (SPP), which allocates containers to individual slots [Pacino *et al.*, 2011]. However, these subproblems in representative form, particularly the MPP, remain non-trivial and difficult to solve especially in the presence of uncertainty [Van Twiller *et al.*, 2024b].

## 1 Introduction

In recent years, machine learning (ML) for combinatorial optimization (CO) has gained much traction [Bengio *et al.*, 2021]. Learning advanced planning policies yields promising results in solving CO problems in transportation and logistics. Such approaches can outperform existing solution methods in some well-known problems, such as vehicle routing [Kool *et al.*, 2019; Hottung *et al.*, 2022] or job shop scheduling [Kwon *et al.*, 2020]. Even though it is important to benchmark algorithms on traditional CO problems, a significant opportunity

In addition to its complexity, stowage planning faces public data scarcity and relies heavily on human planners supported by limited decision support systems [Jensen *et al.*, 2018]. Planners should maximize capacity utilization while managing demand uncertainty by accounting for multiple future scenarios. However, evaluating such scenarios is computationally intractable, due to the problem's complexity and dynamic nature. These limitations highlight the need for efficient, adaptive, and feasible decision-support systems, offering an opportunity for AI-driven solution methods to enhance the resilience and sustainability of the global supply chain.

\*This paper is currently under review for IJCAI 2025.

This paper presents a deep reinforcement learning (DRL) approach with feasibility projection to construct adaptive and feasible solutions, providing a decision-support policy for the MPP under demand uncertainty.

Our main contributions are as follows:

- **Master Stowage Planning Environment:** We develop a novel Markov decision process (MDP) for master stowage planning under demand uncertainty, incorporating realistic problem-specific constraints. To address data scarcity, we release the environment as an open-source implementation<sup>1</sup>.
- **Feasibility Projection:** We incorporate differentiable projection layers, including weighted scaling, policy clipping, and violation projection, to enforce inequality constraint satisfaction in DRL frameworks.
- **Efficient and Adaptive Solutions:** Our experiments demonstrate that our policy efficiently generates adaptive and feasible solutions under demand uncertainty, significantly outperforming well-known DRL methods and a multi-stage stochastic MIP model.
- **Decision Support for Stowage Planning:** Our decision-support policy transcends deterministic models, enabling dynamic and uncertainty-informed planning in a critical part of the global supply chain.

## 2 Domain Preliminaries

We present the preliminaries of the stowage planning domain to provide the planning context. We refer to [Jensen *et al.*, 2018] for a comprehensive review.

**Voyages.** Liner shipping companies utilize fleets of container vessels that operate on fixed schedules along a closed-loop course, similar to a maritime bus service that carries goods between ports. The complete journey covering all ports is called a voyage, typically starting in regions with a supply surplus (e.g., Asia) and navigating towards high-demand discharge areas (e.g., Europe), often voyages cover more than ten ports. A voyage can be described as a directed path graph  $G_P = (P, E_P)$  with nodes being  $P = \{1, 2, \dots, N_P\}$ , and edges being legs between ports  $E_P = \{(p, p+1) \mid p \in \{1, 2, \dots, N_P-1\}\}$  with  $N_P$  being the last port. We also define sub-voyages by set  $P_{\text{start}}^{\text{end}} = \{p \in P \mid \text{start} \leq p \leq \text{end}\}$ .

Containers have a port of load (*pol*) and a port of discharge (*pod*), also named transports or origin-destination pairs. Consider  $pol \in P_1^{N_P-1}$  and  $pod \in P_2^{N_P}$  with  $P^2 = P \times P$ , which can be represented by transport  $tr = (pol, pod)$ . We can define a set of transports  $TR = \{(i, j) \in P^2 \mid i < j\}$ .

**Container Cargo.** Containers vary in dimensions and types, but we focus on the most common and impactful characteristics: lengths (20 ft, 40 ft), weight classes (light, medium, heavy), and customer types (long-term, spot market). Container revenue is driven by customer contract types, where *rev* is the revenue depending on cargo type and transport. Long-term contracts provide lower revenue but ensure high, stable volumes, whereas spot market contracts yield

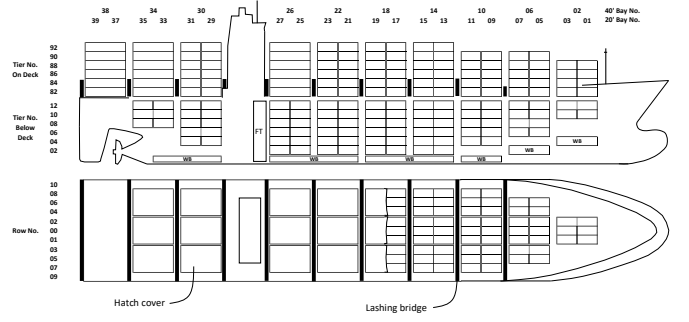


Figure 1: The side and top view of a container vessel.

higher revenue with lower, more volatile volumes. Long-term contracts are prioritized over spot contracts. However, the lack of no-show fees creates inherent uncertainty in container demand, which becomes more predictable as the arrival date approaches. Consequently, planners must dynamically allocate cargo to vessels during the voyage while managing uncertainty. Containers are often grouped into cargo classes by characteristics, such as  $K = \{20ft, 40ft\} \times \{Light, Medium, Heavy\} \times \{Spot, Long\}$ .

**Vessel Layout.** Figure 1 shows the cellular layout of container vessels with standardized coordinates of (*bay*, *row*, *tier*). It is divided into bays (02-38) ranging from the front (e.g., bay 02) to the rear (e.g., bay 38), also named from fore to aft. Bays are defined by an ordered set  $B = \{1, 2, \dots, N_B\}$ , ranging from fore to aft with  $N_B$  being the last bay. Each bay contains stacks of cells, whereas cells contain two slots that can hold two 20-foot containers or one 40-foot container. Bays are horizontally separated by hatch covers into above and below deck sections, introducing the set of decks  $D = \{d^{above}, d^{below}\}$ . It is worth noting that hatch covers introduce complexity since below-deck cargo can only be discharged if the above-deck cargo is cleared.

**Utilization.** Vessel utilization  $u_p \in \mathbb{Z}^{|B| \times |D| \times |K| \times |TR|}$  represents the cargo placement across bays  $B$ , decks  $D$ , cargo types  $K$ , and transports  $TR$ . Load operations are defined by  $u_p^+ \in \mathbb{Z}_{\geq 0}^{|B| \times |D| \times |K| \times |TR|}$ , whereas discharging is denoted by  $u_p^- \in \mathbb{Z}_{\geq 0}^{|B| \times |D| \times |K| \times |TR|}$ . The utilization at port  $p$  is defined as  $u_p = u_{p-1} + u_p^+ - u_p^- \forall p \in P$ , where  $u_0$  is the vessel's arrival condition at the first port. We also define the vessel's pre-loading utilization  $u_p^- = u_{p-1} - u_p^-$ .

**Objectives and Global Constraints.** The MPP aims to create a capacity management plan for each general location (indexed by bay and deck) while adhering to global constraints, as outlined below. The MPP maximizes revenue by optimizing capacity for high-value cargo and minimizes costs through improved operational efficiency. The SPP then assigns containers to slots within the general locations while considering local constraints. Due to frequent re-planning as new information arises, algorithmic runtimes over 10 minutes are impractical for real-world operations [Pacino *et al.*, 2011].

Vessels have different types of capacity related to TEUs, height, weight and special cargo. The amount to which this can be utilized depends on the arrival condition of vessels

<sup>1</sup>[https://github.com/OptimalPursuit/navigating\\_uncertainty\\_in\\_mpp](https://github.com/OptimalPursuit/navigating_uncertainty_in_mpp)

and uncertain cargo demand. It is therefore non-trivial to ensure optimal utilization of vessel capacities. The key efficiency objectives are minimizing overstockage, an NP-hard task [Tierney *et al.*, 2014], and minimizing the quay crane makespan. Overstockage occurs when containers stacked on top block access to those below in need of discharging, requiring additional crane operations to remove and reload the obstructing containers, thereby increasing the workload. In addition, the crane makespan considerably impacts the port stay duration, while ports set makespan targets and overruns incur costs. It is thus beneficial to minimize the makespan by maximizing the average use of parallel cranes, thereby minimizing idle time.

Furthermore and most importantly, vessels must adhere to safety requirements to ensure seaworthiness, which is heavily influenced by weight distribution. Before introducing the constraints, we first clarify that  $\otimes$  represents the outer product and  $\odot$  denotes the element-wise Hadamard product, with broadcasting applied when shapes are compatible. The longitudinal ( $lcg$ ) and vertical centres of gravity ( $vcg$ ), which are associated with trim and metacentric height, of the load  $u_p$  prior to leaving port  $p$  must remain within specified bounds ( $lcg, \overline{lcg} \in \mathbb{R}_{>0}$ ), as shown in Constraints (1) and (2). To compute the stability, we define the longitudinal moment  $lm = ld \otimes w$  and vertical moment  $vm = vd \otimes w$ , where  $w \in \mathbb{R}_{>0}^{|K| \times |TR|}$  represents container weights, and  $ld, vd \in \mathbb{R}^{|B| \times |D|}$  denote the longitudinal and vertical distances of positions from the vessel's centre of gravity.

$$\overline{lcg} \leq \frac{\mathbf{1}^\top (lm \odot u_p)}{\mathbf{1}^\top (w \odot u_p)} \leq \overline{lcg}, \quad \forall p \in P \quad (1)$$

$$\overline{vcg} \leq \frac{\mathbf{1}^\top (vm \odot u_p)}{\mathbf{1}^\top (w \odot u_p)} \leq \overline{vcg}, \quad \forall p \in P \quad (2)$$

In conclusion, the scale and complexity of the problem pose significant challenges. As a result, most models focus on subsets of realistic constraints to remain tractable, often requiring human intervention to ensure practical usability.

### 3 Related Work

This section positions our work in the literature on stowage planning, stochastic programming and ML in optimization.

**Stowage Planning.** To address the complexity of stowage planning, various solution approaches have been applied to different problem formulations, including exact methods [Roberti and Pacino, 2018], linearly relaxed MIP [Pacino *et al.*, 2011], matheuristics [Parreño-Torres *et al.*, 2021], population-based metaheuristics [Chang *et al.*, 2022], neighbourhood-based metaheuristics [Pacino, 2018], hybrid frameworks [Bilican *et al.*, 2020]. Despite these techniques, a recent survey highlights that scalable solutions for representative stowage and MPP problems remain unsolved [Van Twiller *et al.*, 2024b]. Research has largely focused on deterministic problems, overlooking real-world needs for profit maximization in the face of demand uncertainty.

**Stochastic Programming.** Decision-making under uncertainty is traditionally approached through stochastic programming, where uncertainty is explicitly represented as a set

of discrete scenarios evolving over multiple stages in time, approximating the underlying probability distribution [Birge and Louveaux, 2011]. This process results in a scenario tree, whose computational complexity grows exponentially as  $\mathcal{O}(b^T)$ , where  $b$  is the branching factor and  $T$  is the number of stages. Hence, multi-stage problems with  $T > 2$  and a reasonably large  $b$  are often intractable. Common techniques to overcome this complication are scenario reduction to reduce problem size [Römis, 2009], decomposition techniques like Benders decomposition or Lagrangian relaxation to divide the problem [Rahmaniani *et al.*, 2017], progressive hedging to enforce non-anticipativity iteratively [Boland *et al.*, 2018], or approximation methods, such as stochastic dual dynamic programming [Shapiro, 2011] and sample average approximation [Chen and Luedtke, 2022], to enhance tractability while preserving solution quality.

**Learning with Hard Constraints.** In learning solution heuristics, a challenge arises to ensure feasibility in complex action spaces. This challenge is exacerbated when dealing with the dependence on state variables to define the feasible region. Several deep learning approaches have dealt with learning constraints by backpropagation through (in)equality completion [Donti *et al.*, 2021], or differentiable projection layers, such as mapping interior points to boundaries [Li *et al.*, 2023], convex programming layers [Agrawal *et al.*, 2019], or problem-specific repair layers [Chen *et al.*, 2024]. Moreover, safe reinforcement learning has dealt with constraints by, e.g., constrained MDPs with a primal-dual approach [Ding *et al.*, 2020], soft barriers function [Wang *et al.*, 2023], and safety shields [Alshiekh *et al.*, 2018].

## 4 Markov Decision Processes

We present a formal MDP and a decomposed MDP to solve using DRL approaches. Technical details about both MDPs are provided in Appendix A.

### 4.1 Formal MDP

Let  $\mathcal{M} = (S, X, \mathcal{T}, \mathcal{R}, P_1^{N_P-1}, \gamma)$  define an episodic discounted MDP representing the MPP, where  $S$  is a set of states,  $X$  is a set of actions,  $\mathcal{T} : S \times X \rightarrow \Delta(S)$  is the transition function,  $\mathcal{R} : S \times X \times P_1^{N_P-1} \rightarrow \mathbb{R}$  is the reward function,  $P_1^{N_P-1}$  is the finite horizon of load ports with  $N_P - 1$  being the last port, and  $\gamma \in (0, 1]$  is the discounting factor.

**State.** The state is given by  $s_p \in S$ , defined as  $s_p = (u_p, q_p, \zeta)$ . This includes vessel utilization  $u_p \in \mathbb{R}_{\geq 0}^{n_u}$  and realized demand  $q_p \in \mathbb{R}_{\geq 0}^{n_q}$ , where  $n_u = |B| \times |D| \times |K| \times |TR|$ ,  $n_c = |B| \times |D|$  and  $n_q = |K| \times |TR|$  are the shapes of utilization, location and demand, respectively.

Additionally, environment parameters  $\zeta$  contain the expected value  $\mu \in \mathbb{R}_{\geq 0}^{n_q}$  and standard deviation  $\sigma \in \mathbb{R}_{\geq 0}^{n_q}$  of demand, load ports  $i$ , discharge ports  $j$  and cargo types  $k$  as  $(i, j, k) \in TR \times K$ , TEU per container  $teu \in \{1, 2\}^{n_q}$ , cargo weight  $w \in \mathbb{R}_{>0}^{n_q}$ , cargo revenue  $rev \in \mathbb{R}_{>0}^{n_q}$ .

The initial state  $s_0 = (u_0, q_0, \zeta)$  consists of an empty vessel  $u_0 = \mathbf{0}^{n_u}$ , realized demand  $q_0$  at initial port, and  $\zeta$  is initialized randomly for each episode.

**Action.** An action  $x_p \in X$  assigns a real number of containers to utilization  $u_p$ , where  $x_p \in \mathbb{R}_{>0}^{n_u}$  and thus similar

to  $u_p^+$ . Each action  $x_p$  is subject to a feasible region, defined by polyhedron  $PH(s_p) = \{x_p \in \mathbb{R}_{\geq 0}^{n_u} : A(s_p)x_p \leq b(s_p)\}$ . Here,  $A(s_p) \in \mathbb{R}^{m_u \times n_u}$  is the constraint matrix,  $b(s_p) \in \mathbb{R}^{m_u}$  is the bound vector, and  $m_u$  is the number of constraints.

Previous work demonstrated that linearly relaxed MPPs outperform exact MPPs, as the subsequent SPP effectively discretizes the solution [Pacino *et al.*, 2011]. Accordingly, we can adopt real-valued actions instead of integer-valued actions. Given a traditional MPP formulation with utilization  $u_p$  [Van Twiller *et al.*, 2024a], we define constraints of  $PH(s_p)$  in terms of actions  $x_p$  and pre-loading utilization  $u'_p$ .

$$x_p^\top \mathbf{1}_{n_c} \leq q_p \quad (3)$$

$$x_p^\top \mathbf{1}_{n_c} \leq c - u'_p \quad (4)$$

$$-\mathbf{1}^\top((lm - lcgw) \odot x_p) \leq -\mathbf{1}^\top((lcgw - lm) \odot u'_p) \quad (5)$$

$$\mathbf{1}^\top((lm - lcgw) \odot x_p) \leq \mathbf{1}^\top((lcgw - lm) \odot u'_p) \quad (6)$$

$$-\mathbf{1}^\top((vm - vcgw) \odot x_p) \leq -\mathbf{1}^\top((vcgw - vm) \odot u'_p) \quad (7)$$

$$\mathbf{1}^\top((vm - vcgw) \odot x_p) \leq \mathbf{1}^\top((vcgw - vm) \odot u'_p) \quad (8)$$

Constraint (3) limits load  $x_p$  to the available demand  $q_p$ , while Constraint (4) ensures  $x_p$  does not exceed the residual TEU capacity. Constraints (5)–(6) enforce lcg limits, while Constraints (7)–(8) impose similar bounds on the vcg. These stability bounds are derived from Constraints (1) and (2).

**Transition.** We use a stochastic transition function  $\mathcal{T}(s_{p+1}|s_p, x_p) \in \Delta(S)$ . Within an episode, the transition consists of multiple components:

- Upon port arrival, port demand  $q_p$  is revealed.
- Subsequently, onboard cargo is discharged  $u_{p+1} = u_p \odot (1 - e_p^-)$ , where  $e_p^- \in \{0, 1\}^{n_q}$  is a binary mask indicating the cargo type and transport to nullify in  $u_p$ .
- Finally, cargo is loaded onboard  $u_{p+1} = u_p + x_p$ . Action  $x_p$  is based on the current utilization  $u_p$  and revealed demand  $q_p$  of port  $p$ . Future port demand stays unknown.

**Reward.** Equation (9) defines our deterministic reward function, computing profit as the difference between revenue and costs. Revenue is computed as the sum of  $x_p$  corresponding to elements of  $q_p$ . Since revenue cannot be obtained from containers exceeding demand, the summation of  $x_p$  is restricted to the elements within  $q_p$ . While costs are computed via the state-dependent auxiliary variables hatch overflows  $ho(s_p, p) \in \mathbb{R}_{>0}^{|B|}$  and excess crane moves  $cm(s_p, p) \in \mathbb{R}_{>0}^{|B|-1}$ . These costs are weighted by  $ct^{ho} \in \mathbb{R}_{>0}$  and  $ct^{cm} \in \mathbb{R}_{>0}$ , respectively.

$$\mathcal{R}(s, x, p) = rev \min(x^\top \mathbf{1}_{n_c}, q) - ct^{ho} \mathbf{1}^\top ho(s, p) + ct^{cm} \mathbf{1}^\top cm(s, p). \quad (9)$$

## 4.2 Decomposed MDP

The formal MDP defines an effective action space of size  $|X| \propto |B| \cdot |D| \cdot |K| \cdot |P|$ , where each action  $x_p$  determines how cargo types and transport options are placed on the vessel per port. However, this action space is large, which can hinder learning efficiency [Kanervisto *et al.*, 2020].

To address this, we decompose the formal MDP into granular, sequential steps based on an index  $(i, j, k) \forall (i, j) \in TR, k \in K$ . Instead of placing all transport and cargo types simultaneously, we take a decomposed action for all transports  $(p, j)$  and cargo types  $k$  at port  $p$ , then departing to a new port. This reduces the action space to  $|X| = |B| \cdot |D|$ , while unfolding transports and cargo types over an extended time horizon  $t \in H = \{0, 1, \dots, T_{seq}\}$  with  $T_{seq} = |K| \cdot |TR|$ .

**State.** The state  $s_t = (u_t, q_t, \zeta)$  depends on time step  $t$ , where  $u_t \in \mathbb{R}_{\geq 0}^{n_u}$  is vessel utilization, and  $q_t \in \mathbb{R}_{\geq 0}^{n_q}$  is realized demand. The environment parameter  $\zeta$  remains unchanged. Given the time  $t$ , however, we can extract relevant parameters from  $\zeta$ , such as  $(pol_t, pod_t, k_t)$ ,  $rev^{(pol_t, pod_t, k_t)}$ .

**Action.** Action  $x_t \in \mathbb{R}_{\geq 0}^{n_c}$  assigns real number of containers to utilization  $u_t$  for step  $t$ . Each action is subject to  $PH(s_t) = \{x_t \in \mathbb{R}_{\geq 0}^{n_c} : A(s_t)x_t \leq b(s_t)\}$ . Here,  $A(s_t) \in \mathbb{R}^{m_c \times n_c}$  is the constraint matrix,  $b(s_t) \in \mathbb{R}^{m_c}$  is the bound vector, and  $m_c$  is the number of constraints. It is also worth noting that Constraints (3)–(8) are reformulated to fit feasible region  $PH(s_t)$ .

**Transition.** At each time step  $t$ , the transition includes loading, where  $x_t$  is added to  $u_t$ . However, discharging and demand realization occur only when arriving at a new port, indicated by  $t \in T_{new \text{ port}}$ .

**Reward.** The revenue at step  $t$  is computed as  $rev^{(pol_t, pod_t, k_t)} \min(\mathbf{1}^\top x_t, q_t^{(pol_t, pod_t, k_t)})$ . However, costs depend on knowing all loading operations at port  $p$ , which is aggregated in utilization  $u_t$  at the last step of the port  $t \in T_{leave \text{ port}}$ . As a result, the cost signal is sparse, being evaluated only once per port  $p$ , rather than at each step.

## 5 Proposed Architecture

Our approach consists of several components: an encoder-decoder model parameterized by  $\theta$ , an actor-critic DRL method, and a feasibility projection layer. The encoder-decoder model shown in Figure 2 employs a look-ahead policy  $\pi_\theta(x|s_t)$  conditioned on state  $s_t$  and parameterized by mean  $\mu_\theta(s_t)$  and standard deviation  $\sigma_\theta(s_t)$ . By training in the decomposed MDP and optionally projecting the policy, we iteratively generate actions  $x_t$  to construct solutions.

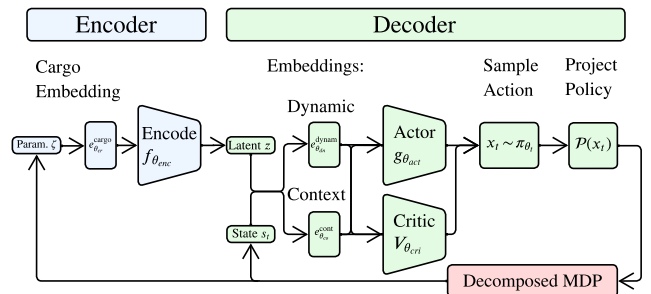


Figure 2: Deep Reinforcement Learning Architecture with Feasibility Projection for Actor-Critic Methods

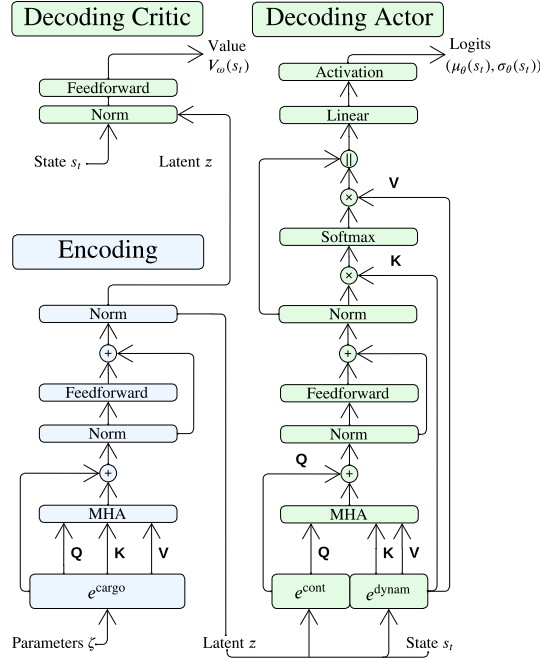


Figure 3: Layers of the encoder and the actor-critic decoder.

### 5.1 Encoder-Decoder Model

Figure 3 presents our encoder-decoder model, based on that of [Kool *et al.*, 2019], with modifications highlighted below.

**Cargo Embedding.** The cargo embedding  $e^{\text{cargo}}(\zeta)$  parameterized by  $\theta_{cr}$  maps cargo-related episode information in  $\zeta$  into a feature representation for the encoder. To enhance positional awareness, we subsequently apply sinusoidal positional encoding [Vaswani *et al.*, 2017].

**Encoding Layers.** An attention encoder  $f(e^{\text{cargo}}(\zeta))$  parameterized by  $\theta_{enc}$  maps embedding  $e^{\text{cargo}}(\zeta)$  to latent variable  $z$  using multi-head attention (MHA) to identify relevant features dynamically [Vaswani *et al.*, 2017]. Then, we use a feed-forward network (FFN) with ReLU activation, layer normalization, residual connections, and dropout.

**Context Embedding.** The context embedding  $e^{\text{cont}}(u_t, z)$ , parameterized by  $\theta_{co}$ , focuses on time  $t$ , extracting time-specific features from the utilization  $u_t$  and latent variable  $z$ . These features provide the MHA query with a representation of the vessel’s current condition, enabling the policy to make decisions based on the present context.

**Dynamic Embedding.** The dynamic embedding  $e^{\text{dynam}}(q_t, z)$ , parameterized by  $\theta_{dn}$ , extracts features from demand  $q_t$  in all steps of horizon  $H$ , capturing patterns across the entire episode. It combines real demand and latent information to produce keys and values for the MHA layer. As such, it accounts for global temporal trends, allowing it to anticipate future conditions and make long-term decisions.

**Actor Layers.** As proposed in [Kool *et al.*, 2019], our actor decoder  $g(e^{\text{cont}}(u_t, z), e^{\text{dynam}}(q_t, z))$  is an attention model parameterized by  $\theta_{act}$ . However, our actor takes input from the context and dynamic embedding. An MHA layer with a forward-looking mask bases decisions on steps

$t, t + 1, \dots, T_{seq}$  to anticipate future events. Subsequently, an FFN extracts features, after which a pointer mechanism performs a soft selection of relevant steps using key-value inputs [Vinyals *et al.*, 2015]. A softplus activation outputs positive logits  $(\mu_\theta(s_t), \sigma_\theta(s_t))$ .

**Critic Layers.** Our critic model  $V(s_t, z)$ , parameterized by  $\theta_{cri}$ , estimates the value of state  $s_t$  and latent variable  $z$  through an FFN outputting  $V_{\theta_{cri}}(s_t, z) \in \mathbb{R}$ .

**Action Policy.** The actor logits parameterize a stochastic policy  $\pi_\theta(x|s_t) = \mathcal{N}((\mu_\theta(s_t), \sigma_\theta(s_t)))$ , which allows action sampling  $x_t \sim \pi_\theta(x|s_t)$  to construct solutions.

### 5.2 Feasibility Regularization in Actor-Critic Loss

Standard actor-critic methods can efficiently and stably learn policies that require implicit feasibility in the action space [Schulman *et al.*, 2017; Haarnoja *et al.*, 2018], while explicit constraints are often integrated by feasibility regularization (FR) in the actor loss [Ding *et al.*, 2020; Calvo-Fullana *et al.*, 2021]. Equation (11) defines a composite loss that combines the actor loss  $\mathcal{L}_{\text{actor}}(\theta)$  with a soft regularization term  $\mathcal{L}_{\text{feas}}(\theta)$ . FR is defined in Equation (11), where  $\lambda_f$  controls the regularization strength, and policy samples  $x_\theta(s_t)$  are assumed to allow gradient flow to update parameters  $\theta$ , as is the case in SAC [Haarnoja *et al.*, 2018]. For algorithms that do not include actions in the computation graph, e.g., PPO [Schulman *et al.*, 2017], we substitute  $x_\theta(s_t)$  with  $\mu_\theta(s_t)$ .

Determining Lagrangian multipliers ( $\lambda_f$ ) for multiple constraints with varying scales is already challenging for static feasible regions. It requires costly hyperparameter tuning to balance a trade-off between objectives and feasibility effectively. As a result, FR is a naive approach when applied to dynamic, state-dependent feasible regions  $PH(s_t)$  [Calvo-Fullana *et al.*, 2021; Donti *et al.*, 2021]. However, FR remains useful as a comparative baseline.

$$\mathcal{L}(\theta) = -\mathcal{L}_{\text{actor}}(\theta) + \lambda_f \mathcal{L}_{\text{feas}}(\theta) \quad (10)$$

$$\mathcal{L}_{\text{feas}}(\theta) = \mathbb{E}_t \left[ (\max(A(s_t)x_\theta(s_t) - b(s_t))_{>0})^2 \right] \quad (11)$$

### 5.3 Feasibility Layers

To extend beyond FR, we leverage differentiable projection layers for constraint minimization. We incorporate two constraint-specific and one general layer(s). Note that a single action may be infeasible while combining such actions can achieve feasibility. Therefore, we prioritize violation minimization over strict enforcement to allow for flexibility.

Furthermore, non-linear transformations of continuous distribution samples change their probability density. We account for this transformation using Jacobian adjustments to the policy’s log probabilities [Bishop, 2006].

Technical details on feasibility layers are provided in Appendix B of supplementary material.

**Weighted Scaling Projection.** Function (12) defines the weighted scaling layer (WS), which normalizes vector  $x$  if the sum of  $x$  exceeds scalar  $y$ . This preserves relative proportions of elements in  $x$  while enforcing  $x$  to sum to scalar  $y$ .

$$\mathcal{W}(x, y) = \begin{cases} y \frac{x}{\mathbf{1}^\top x} & \text{if } \mathbf{1}^\top x > y \\ x & \text{otherwise} \end{cases} \quad (12)$$

---

**Algorithm 1** Violation Projection Layer

---

**Require:**  $x \in \mathbb{R}_{>0}^n$ , parameters  $(A, b, \eta_v, \delta_v)$

```
1: Initialize  $x' \leftarrow x$ 
2: Define  $\mathcal{V}(x) \leftarrow (Ax - b)_{>0}$ 
3: for  $i = 1$  to epochs do
4:   Set  $x \leftarrow x'$ 
5:   Update  $x' \leftarrow x - \eta_v A^\top \mathcal{V}(x)$ 
6:   if  $\mathbf{1}^\top \mathcal{V}(x') - \mathbf{1}^\top \mathcal{V}(x) \leq \delta_v$  then
7:     break
8:   end if
9: end for
10: return  $x'$ 
```

---

**Policy Clipping.** We can apply function  $\mathcal{C}(x, lb_{pc}, ub_{pc}) = \max(\min(x, ub_{pc}), lb_{pc})$  to enforce element-wise limits on vector  $x$ , thereby performing policy clipping (PC) on actions. However, PC is only applicable to box constraints.

**Violation Projection.** In Algorithm 1, we define a violation projection (VP) layer that reduces inequality constraint violations by shifting point  $x$  closer to the feasible region of some convex polyhedron  $PH = \{x \in \mathbb{R}_{>0}^n : Ax \leq b\}$ , where  $A \in \mathbb{R}^{m \times n}$  and  $b \in \mathbb{R}^m$ . The inequality  $Ax \leq b$  ensures  $PH$  is convex, enabling gradient-based reduction of violation  $\mathcal{V}(x)$  [Boyd and Vandenberghe, 2004]. To measure feasibility, we compute the element-wise violation  $\mathcal{V}(x) = (Ax - b)_{>0}$ , where each  $\mathcal{V}(x)_{m_i} > 0$  indicates the violation of constraint  $m_i$ , and  $\mathcal{V}(x)_{m_i} = 0$  indicates satisfaction of that constraint. To minimize violations, we iteratively update  $x$  by applying gradient descent to reduce the violation term  $\|\mathcal{V}(x)\|_2^2$ , representing the squared distance from  $x$  to  $PH$ . Equation (13) updates  $x$  with a step size  $\eta_v$ , which is rewritten to the update function found in Algorithm 1.

$$x' = x - \eta_v \nabla_x \|\mathcal{V}(x)\|_2^2 \quad (13)$$

During training, the VP layer continues for a fixed number of epochs. However, we include a stopping criteria during inference, which continues until the change in total violation  $\mathbf{1}^\top \mathcal{V}(x') - \mathbf{1}^\top \mathcal{V}(x)$  is below a threshold  $\delta_v$ . As a result, we  $x$ 's distance to the feasible region and incorporate constraint awareness into initially unconstrained policies.

## 6 Experimental Results

We compare our policies against baselines on in-distribution and out-of-distribution instances, evaluating the objective value, computational cost and feasibility. Additionally, an ablation study analyzes the impact of feasibility mechanisms and gradient flow from actions, while managerial insights discuss the value of information, computational cost, and adaptiveness to varying levels of uncertainty.

### 6.1 Experimental Setup

**Instance Generation.** Training instances are sampled from a Gaussian distribution  $\mathcal{N}(\mu^{(i,j,k)}, \sigma^{(i,j,k)}) \forall (i, j) \in TR, k \in K$ , where  $\mu^{(i,j,k)}$  is randomly generated and  $\sigma^{(i,j,k)} = CV\mu^{(i,j,k)}$  controls spread via the coefficient of variation  $CV$ . A continuous uniform distribution generates out-of-distribution instances  $\mathcal{U}(lb^{(i,j,k)}, ub^{(i,j,k)}) \forall (i, j) \in TR, k \in K$  to test generalization. Details are in Appendix C.

**Feasibility Implementation.** We evaluate feasibility by integrating multiple mechanisms to address all constraints in  $PH(s_t)$ . Starting with a baseline using FR, we introduce two alternatives: a constraint-specific (FR/WS/PC) and a general projection approach (FR/VP). We then remove FR from both to assess its impact. WS and PC are not analyzed separately, as it leaves many constraints unaddressed.

**SMIP Baseline.** We compare our approach against two common techniques in stochastic programming: SMIP-NA (stochastic MIP without anticipation) and SMIP-PI (stochastic MIP with perfect foresight, serving as an upper bound). The scenario trees and MIP models are shown in Appendix D.

**Runs.** Training occurs offline on simulated instances for a 1,000 TEU vessel over a 4-port voyage. GPU-based experiments use an NVIDIA RTX A6000, and CPU-based runs use an AMD EPYC 9454 48-core processor. Implementation details and additional experiments are provided in Appendix E.

### 6.2 Policy Performance

Table 1 compares the performance of different solution approaches. Our projected attention models (AM-P) outperform SMIP-NA, achieving around 30-35% higher objective values and 500x faster computations. The AM with FR misleadingly attains higher profits than SMIP-NA due to infeasibility. If we recover feasibility, then profits are significantly reduced to the level of SMIP-NA. In contrast, each AM-P finds feasible solutions with a higher profit than AM with FR, highlighting FR's limitations. All AM-P policies generalize well, with SAC and PPO showing an average profit reduction of 2% and 3% on unseen uniform instances, similar to SMIP-NA and SMIP-PI. These results suggest that AM-P can leverage imperfect information to anticipate future uncertainty and ensure feasibility by projection layers beyond FR.

**Ablation Study.** Table 1 analyzes the impact of feasibility mechanisms. Removing FR from FR/VP increases profit for SAC and slightly decreases profit for PPO, without diminishing feasibility. When FR is removed from FR/WS/PC, profit increases, and both DRL approaches continue to maintain feasibility. This outcome is surprising, given the absence of a direct mechanism to account for stability. However, from our domain understanding, we know container vessels generally become more stable as utilization increases in all locations. Replacing SAC with PPO, which eliminates action gradient flow, reduces feasibility in FR, though projection layers mitigate this effect. These findings highlight the impact of feasibility mechanisms on the objective value and feasibility.

### 6.3 Managerial Insights

Figure 4 performs a sensitivity analysis to examine the effects of SMIP scenario size and demand uncertainty, reporting with an average and 95% confidence interval (CI).

**Value of Information.** Figure 4a compares performance under non-anticipation, imperfect, and perfect information. The predictive accuracy of SMIP models improves with the number of scenarios, as shown by the stabilizing yet decreasing objective values. With 28 scenarios, perfect information enhances profit by 60-65%, while imperfect information via DRL with VP achieves a 25-40% improvement, emphasizing the role of information availability for decision quality.



Methods			Testing ( $N = 30$ )				Generalization ( $N = 30$ )			
Alg.	Model	F.M.	Ob. (\$)	Time (s)	F.I. (%)	F.O. (\$)	Ob. (\$)	Time (s)	F.I. (%)	F.O. (\$)
SAC	AM	FR	1113.03 <sup>†</sup>	12.63	0.00	1065.80	1211.87 <sup>†</sup>	15.35	0.00	1041.42
SAC	AM-P	FR/VP	1318.05	15.20	100.00	-	1288.68	14.18	100.00	-
SAC	AM-P	VP	1447.69	15.03	100.00	-	1411.34	13.33	100.00	-
SAC	AM-P	FR/WS/PC	1373.24	13.34	100.00	-	1340.12	14.42	100.00	-
SAC	AM-P	WS/PC	1494.22	13.12	100.00	-	1482.40	12.91	100.00	-
PPO	AM	FR	1842.46 <sup>†</sup>	11.74	0.00	1063.24	1830.95 <sup>†</sup>	12.60	0.00	1066.69
PPO	AM-P	FR/VP	1355.45	15.60	100.00	-	1321.90	14.91	100.00	-
PPO	AM-P	VP	1318.10	14.51	100.00	-	1282.10	14.64	100.00	-
PPO	AM-P	FR/WS/PC	1369.03	14.29	100.00	-	1330.10	14.17	100.00	-
PPO	AM-P	WS/PC	1471.40	13.75	100.00	-	1455.98	13.21	100.00	-
CPL	SMIP-NA	-	1053.02	8434.58	100.00	-	1023.04	8434.94	100.00	-
CPL	SMIP-PI*	-	1713.73	40.75	100.00	-	1680.51	38.93	100.00	-

Table 1: Experimental results comparing DRL methods (SAC/PPO) with a vanilla (AM) or projected attention model (AM-P) and feasibility mechanisms (F.M.): feasibility regularization (FR), weighted scaling (WS), policy clipping (PC) and violation projection (VP). We compare SMIP-NA (non-anticipation) as a baseline, and SMIP-PI (\* assumes perfect information which is unrealistic) as an expected upper bound, both solved with CPLEX (CPL). Average performance metrics on  $N$  instances include objective value in profit (Ob.), inference time in seconds (Time), percentage of feasible instances (F.I.), and objective value with feasibility recovery (F.O.). Note that <sup>†</sup> indicates infeasible objectives. Generalization performance is evaluated on unseen, out-of-distribution instances based on a uniform distribution.

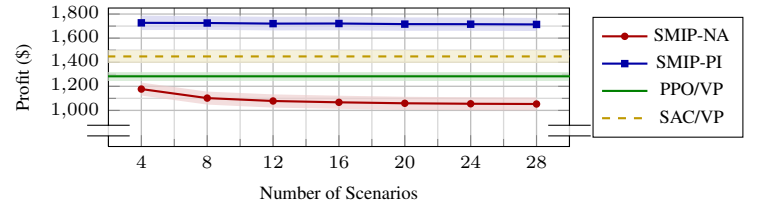
**Computational Time.** While inference time is critical, training time remains relevant. Figure 4b illustrates the total computational time of 30 instances, with training time included for DRL. Computational cost increases significantly with the number of scenarios, with SMIP-NA exhibiting exponential growth and SMIP-PI showing steady growth. Solving the most accurate SMIP-NA takes approximately 2 hours per instance, which is intractable for stowage planners. In contrast, the DRL approach requires offline training of about 11 hours, after which solutions can be constructed in seconds.

**Adaptiveness.** Figure 4c illustrates how policies adapt to variations in the spread of the demand distribution of unseen instances. As variability and uncertainty increase, both SAC and PPO policies achieve higher profits, demonstrating their ability to leverage uncertainty. Despite fluctuations in variability, both policies consistently generate feasible solutions.

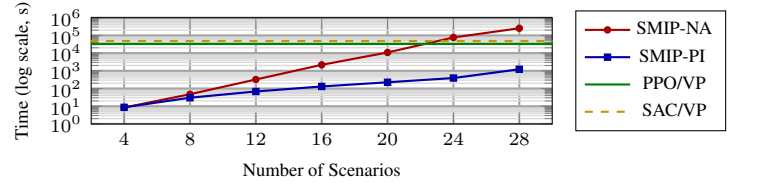
**Implications for Practical Deployment.** Our findings are based on simulations, limited by the lack of real-world data. To ensure effective deployment, practitioners should focus on collecting and generating representative cargo demand data.

## 7 Conclusion and Future Directions

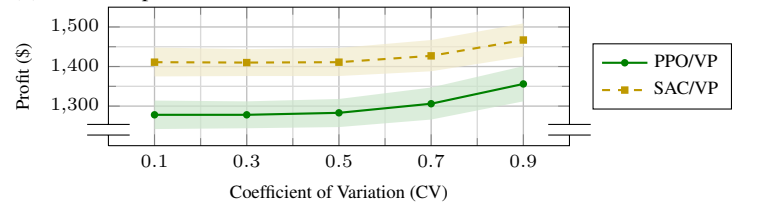
This work introduces a novel MDP formulation for the MPP under demand uncertainty, incorporating realistic inequality constraints. We train an AM policy using actor-critic DRL methods with differentiable feasibility projections to construct MPP solutions. Experimental results demonstrate that our policy efficiently generates adaptive and feasible solutions, significantly outperforming baseline DRL methods and the SMIP-NA. This approach establishes an AI-driven decision-support policy for planning under uncertainty in a critical part of the global supply chain. Future work will extend the MPP formulation and scale to larger vessels and longer voyages, further enhancing the representativeness.



(a) Profit with 95% CI across scenario sizes on 30 instances.



(b) Total computational time across scenario sizes of 30 instances.



(c) Profit with 95% CI across CV levels on 30 unseen instances.

Figure 4: Sensitivity analysis of scenario size and demand spread.

## Ethical Statement

Human oversight is critical in decision-support tools to ensure fairness, accountability, and transparency. While models can enhance decision-making, they must not replace human judgment, particularly in high-stakes applications. We strongly encourage safeguards to mitigate automation bias, ensuring that users can override or challenge outputs, with continuous validation and auditing to uphold trust and fairness.

## References

- [Agrawal *et al.*, 2019] Akshay Agrawal, Brandon Amos, Shane Barratt, and Stephen Boyd. Differentiable Convex Optimization Layers. In *Advances in Neural Information Processing Systems*, 2019.
- [Alshiekh *et al.*, 2018] Mohammed Alshiekh, Roderick Bloem, Rüdiger Ehlers, Bettina Könighofer, Scott Niekum, and Ufuk Topcu. Safe Reinforcement Learning via Shielding. In *Proceedings of the AAAI Conference on Artificial Intelligence*, volume 32, April 2018.
- [Bengio *et al.*, 2021] Yoshua Bengio, Andrea Lodi, and Antoine Prouvost. Machine learning for combinatorial optimization: A methodological tour d’horizon. *European Journal of Operational Research*, 290(2):405–421, April 2021.
- [Bilican *et al.*, 2020] Mevlut Savas Bilican, Ramazan Evren, and Mumtaz Karatas. A Mathematical Model and Two-Stage Heuristic for the Container Stowage Planning Problem with Stability Parameters. *IEEE Access*, 8:113392–113413, 2020.
- [Birge and Louveaux, 2011] J.R. Birge and F. Louveaux. *Introduction to Stochastic Programming*. Springer Series in Operations Research and Financial Engineering. Springer New York, 2011.
- [Bishop, 2006] Christopher M. Bishop. *Pattern recognition and machine learning*. Information science and statistics. Springer, New York, 2006.
- [Boland *et al.*, 2018] Natasha Boland, Jeffrey Christiansen, Brian Dandurand, Andrew Eberhard, Jeff Linderoth, James Luedtke, and Fabricio Oliveira. Combining Progressive Hedging with a Frank–Wolfe Method to Compute Lagrangian Dual Bounds in Stochastic Mixed-Integer Programming. *SIAM Journal on Optimization*, 28(2):1312–1336, January 2018.
- [Boyd and Vandenberghe, 2004] Stephen P. Boyd and Lieven Vandenberghe. *Convex optimization*. Cambridge University Press, Cambridge New York Melbourne New Delhi Singapore, version 29 edition, 2004.
- [Calvo-Fullana *et al.*, 2021] Miguel Calvo-Fullana, Santiago Paternain, Luiz F. O. Chamon, and Alejandro Ribeiro. State Augmented Constrained Reinforcement Learning: Overcoming the Limitations of Learning With Rewards. *IEEE Transactions on Automatic Control*, 69:4275–4290, 2021.
- [Chang *et al.*, 2022] Yimei Chang, Masoud Hamed, and Ali Haghani. Solving integrated problem of stowage planning with crane split by an improved genetic algorithm based on novel encoding mode. *Measurement and Control*, September 2022.
- [Chen and Luedtke, 2022] Rui Chen and James Luedtke. On sample average approximation for two-stage stochastic programs without relatively complete recourse. *Mathematical Programming*, 196(1-2):719–754, November 2022.
- [Chen *et al.*, 2024] Wenbo Chen, Mathieu Tanneau, and Pascal Van Hentenryck. End-to-End Feasible Optimization Proxies for Large-Scale Economic Dispatch. *IEEE Transactions on Power Systems*, 39(2):4723–4734, 2024.
- [Ding *et al.*, 2020] Dongsheng Ding, Kaiqing Zhang, Tamer Basar, and Mihailo Jovanovic. Natural Policy Gradient Primal-Dual Method for Constrained Markov Decision Processes. In H. Larochelle, M. Ranzato, R. Hadsell, M. F. Balcan, and H. Lin, editors, *Advances in Neural Information Processing Systems*, volume 33, pages 8378–8390. Curran Associates, Inc., 2020.
- [Donti *et al.*, 2021] Priya L. Donti, David Rolnick, and J. Zico Kolter. DC3: A learning method for optimization with hard constraints. In *Proceedings of the 9th International Conference on Learning Representations*, April 2021.
- [European Commission, 2023] European Commission. Reducing Emissions from the Shipping Sector, 2023.
- [Fujita and Maeda, 2018] Yasuhiro Fujita and Shin-ichi Maeda. Clipped Action Policy Gradient. In *Proceedings of the 35th International Conference on Machine Learning*, February 2018.
- [Haarnoja *et al.*, 2018] Tuomas Haarnoja, Aurick Zhou, Pieter Abbeel, and Sergey Levine. Soft Actor-Critic: Off-Policy Maximum Entropy Deep Reinforcement Learning with a Stochastic Actor. In *Proceedings of the 35th International Conference on Machine Learning*. PMLR, August 2018.
- [Herup *et al.*, 2022] Mathias Offerlin Herup, Gustav Christian Wichmann Thiesgaard, Jaikje van Twiller, and Rune Møller Jensen. A Linear Time Algorithm for Optimal Quay Crane Scheduling. In *Computational Logistics*, volume 13557, pages 60–73, Barcelona, Spain, 2022. Springer Nature Switzerland.
- [Hottung *et al.*, 2020] André Hottung, Shunji Tanaka, and Kevin Tierney. Deep learning assisted heuristic tree search for the container pre-marshalling problem. *Computers & Operations Research*, 113:104781, 2020.
- [Hottung *et al.*, 2022] André Hottung, Yeong-Dae Kwon, and Kevin Tierney. Efficient Active Search for Combinatorial Optimization Problems. In *Proceedings of the International Conference on Learning Representations*, 2022.
- [Jensen *et al.*, 2018] Rune Møller Jensen, Dario Pacino, Mai Lise Ajspur, and Claus Vesterdal. *Container Vessel Stowage Planning*. Weilbach, 2018.
- [Kanervisto *et al.*, 2020] Anssi Kanervisto, Christian Scheller, and Ville Hautamäki. Action Space Shaping in



- Deep Reinforcement Learning. In *2020 IEEE Conference on Games (CoG)*, May 2020.
- [Kool *et al.*, 2019] Wouter Kool, Herke van Hoof, and Max Welling. Attention, Learn to Solve Routing Problems! In *Proceedings of the International Conference on Learning Representations*, 2019.
- [Kwon *et al.*, 2020] Yeong-Dae Kwon, Jinho Choo, Byoungjip Kim, Iljoo Yoon, Youngjune Gwon, and Seungjai Min. POMO: Policy Optimization with Multiple Optima for Reinforcement Learning. In *Proceedings of the 34th Conference on Neural Information Processing Systems*, 2020.
- [Li *et al.*, 2023] Meiyi Li, Soheil Kolouri, and Javad Mohammadi. Learning to Solve Optimization Problems With Hard Linear Constraints. *IEEE Access*, 11:59995–60004, 2023.
- [Lloyd’s List, 2022] Lloyd’s List. Shipping emissions rise 4.9% in 2021, January 2022.
- [Martin-Iradi *et al.*, 2022] Bernardo Martin-Iradi, Dario Pacino, and Stefan Ropke. The Multiport Berth Allocation Problem with Speed Optimization: Exact Methods and a Cooperative Game Analysis. *Transportation Science*, 56(4):972–999, 2022.
- [Pacino *et al.*, 2011] Dario Pacino, Alberto Delgado, RM Jensen, and Tom Bebbington. Fast generation of near-optimal plans for eco-efficient stowage of large container vessels. *Computational Logistics*, pages 286–301, 2011.
- [Pacino, 2018] Dario Pacino. Crane Intensity and Block Stowage Strategies in Stowage Planning. In *Computational Logistics*, volume 11184 LNCS, pages 191–206. Springer, 2018.
- [Parreño-Torres *et al.*, 2021] Consuelo Parreño-Torres, Hatice Çalık, Ramon Alvarez-Valdes, and Rubén Ruiz. Solving the generalized multi-port container stowage planning problem by a matheuristic algorithm. *Computers and Operations Research*, 133:105383–105383, 2021. Publisher: Elsevier Ltd.
- [Rahmaniani *et al.*, 2017] Ragheb Rahmaniani, Teodor Gabriel Crainic, Michel Gendreau, and Walter Rei. The Benders decomposition algorithm: A literature review. *European Journal of Operational Research*, 259(3):801–817, June 2017.
- [Roberti and Pacino, 2018] R. Roberti and D. Pacino. A decomposition method for finding optimal container stowage plans. *Transportation Science*, 52(6):1444–1462, 2018.
- [Römis, 2009] Werner Römis. Scenario Reduction Techniques in Stochastic Programming. In Osamu Watanabe and Thomas Zeugmann, editors, *Stochastic Algorithms: Foundations and Applications*, volume 5792, pages 1–14. Springer Berlin Heidelberg, Berlin, Heidelberg, 2009. Series Title: Lecture Notes in Computer Science.
- [Schulman *et al.*, 2016] John Schulman, Philipp Moritz, Sergey Levine, Michael I. Jordan, and Pieter Abbeel. High-Dimensional Continuous Control Using Generalized Advantage Estimation. In *4th International Conference on Learning Representations*, 2016.
- [Schulman *et al.*, 2017] John Schulman, Filip Wolski, Prafulla Dhariwal, Alec Radford, and Oleg Klimov. Proximal Policy Optimization Algorithms, July 2017. arXiv:1707.06347.
- [Shapiro, 2011] Alexander Shapiro. Analysis of stochastic dual dynamic programming method. *European Journal of Operational Research*, 209(1):63–72, February 2011.
- [Tierney *et al.*, 2014] Kevin Tierney, Dario Pacino, and Rune Møller Jensen. On the complexity of container stowage planning problems. *Discrete Applied Mathematics*, 169:225–230, 2014.
- [UNCTAD, 2021] UNCTAD. Review of Maritime Transport 2021. Technical report, United Nations, 2021.
- [Van Twiller *et al.*, 2024a] Jaike Van Twiller, Agnieszka Sivertsen, Rune M. Jensen, and Kent H. Andersen. An Efficient Integer Programming Model for Solving the Master Planning Problem of Container Vessel Stowage. In *Computational Logistics*, pages 236–253, Monterrey, Mexico, 2024. Springer Nature Switzerland.
- [Van Twiller *et al.*, 2024b] Jaike Van Twiller, Agnieszka Sivertsen, Dario Pacino, and Rune Møller Jensen. Literature survey on the container stowage planning problem. *European Journal of Operational Research*, 317(3):841–857, 2024.
- [Vaswani *et al.*, 2017] Ashish Vaswani, Noam Shazeer, Niki Parmar, Jakob Uszkoreit, Llion Jones, Aidan N Gomez, Lukasz Kaiser, and Illia Polosukhin. Attention is All you Need. In *Advances in Neural Information Processing Systems*, volume 30. Curran Associates, Inc., 2017.
- [Vinyals *et al.*, 2015] Oriol Vinyals, Meire Fortunato, and Navdeep Jaitly. Pointer Networks. In C. Cortes, N. Lawrence, D. Lee, M. Sugiyama, and R. Garnett, editors, *Advances in Neural Information Processing Systems*, volume 28. Curran Associates, Inc., 2015.
- [Wang *et al.*, 2023] Yixuan Wang, Simon Sinong Zhan, Ruochen Jiao, Zhilu Wang, Wanxin Jin, Zhuoran Yang, Zhaoran Wang, Chao Huang, and Qi Zhu. Enforcing Hard Constraints with Soft Barriers: Safe Reinforcement Learning in Unknown Stochastic Environments. In *Proceedings of the 40th International Conference on Machine Learning*, 2023.

## A MDP of Master Planning Problem

### A.1 Sets and Parameters

Provided the sets and parameters in Section 2, we introduce additional subsets of the transport set  $TR$  given port  $p \in P$ :

- Onboard transports:  $TR_p^{OB} = \{(i, j) \in P^2 \mid i \leq p, j > p\}$
- Arrival transports:  $TR_p^{AC} = \{(i, j) \in P^2 \mid i < p, j > p\}$
- Load transports:  $TR_p^+ = \{(p, j) \in P^2 \mid j > p\}$
- Discharge transports:  $TR_p^- = \{(i, p) \in P^2 \mid i < p\}$
- Transports in crane operations:  $TR_p^M = TR_p^+ \cup TR_p^-$

Considering episode parameters  $\zeta$ , we define:

- Transports:  $tr = (i, j) \in TR$
- Cargo types:  $k = (\kappa_1, \kappa_2, \kappa_3) \in K$

For each combination  $(i, j, k)$ , we associate the expected demand  $\mu^{(i,j,k)}$ , standard deviation  $\sigma^{(i,j,k)}$ , TEU per container  $teu^{(i,j,k)}$ , container weight  $w^{(i,j,k)}$ , and revenue per container  $rev^{(i,j,k)}$ .

The TEU per container depends on  $k$  as:

$$teu(k) = \begin{cases} 1, & \text{if } \kappa_1 = 20 \text{ ft.} \\ 2, & \text{if } \kappa_1 = 40 \text{ ft.} \end{cases}$$

Similarly, the container weight is defined by:

$$w(k) = \begin{cases} 1, & \text{if } \kappa_2 = \text{Light} \\ 2, & \text{if } \kappa_2 = \text{Medium} \\ 3, & \text{if } \kappa_2 = \text{Heavy} \end{cases}$$

The revenue function is given by:

$$rev(i, j, k) = \begin{cases} (j - i)(1 - LR) + 0.1, & \text{if } \kappa_3 = \text{Long} \\ (j - i) + 0.1, & \text{if } \kappa_3 = \text{Spot} \end{cases}$$

The parameters  $\mu$  and  $\sigma$  are randomly generated, as shown in Appendix C.

### A.2 Formal MDP

We define the MDP by decomposing the traditional CO problem outlined in [Van Twiller *et al.*, 2024a].

In the traditional MPP, cargo is loaded onto a vessel at each port in a voyage. Let  $u \in \mathbb{R}^{n_u}$  represent the vessel's utilization over the voyage, which is defined by the set of ports  $P = \{1, 2, \dots, N_P\}$ . Let us also recall the following:

$$n_u = |B| \times |D| \times |K| \times |TR|$$

$$n_c = |B| \times |D|, \quad n_q = |K| \times |TR| \quad n_u = \{n_c \times n_q\}$$

Utilization  $u$  can be decomposed into individual voyage legs, corresponding to the segments between consecutive ports. Specifically, we decompose as:

$$u = (u_0, u_1, \dots, u_{N_P-1})$$

where each  $u_p \in \mathbb{R}^{n_u}$  represents the vessel's utilization immediately after operations at port  $p$ .

### Feasible Region

Suppose we have a feasible region for the MPP, where:

- $A' \in \mathbb{R}^{m_u \times n_u}$  is the constraint matrix,
- $b' \in \mathbb{R}^{m_u}$  is the bound vector,
- $u_p \in \mathbb{R}_{\geq 0}^{n_u}$  is the nonnegative vessel utilization.

The feasible region, denoted as  $PH$ , is given by:

$$PH(s_p) = \{u_p \in \mathbb{R}_{\geq 0}^{n_u} \mid A' u_p \leq b'\}.$$

At port  $p$ , utilization can be decomposed into load operations and pre-load utilization:

$$u_p = u_p' + u_p^+,$$

where:

- $u_p^+ \in \mathbb{R}_{\geq 0}^{n_u}$  represents load operations,
- $u_p' = u_{p-1} - u_p^-$  is the utilization before load operations,
- $u_{p-1} \in \mathbb{R}_{\geq 0}^{n_u}$  is the previous step's utilization,
- $u_p^- \in \mathbb{R}_{\geq 0}^{n_u}$  is the discharge operations.

Consequently, we can rewrite the feasible region as:

$$PH(s_p) = \{u_p^+ \in \mathbb{R}_{\geq 0}^{n_u} \mid A' u_p^+ \leq b' - A' u_p'\}.$$

### A.3 Decomposed MDP

Utilization can be decomposed into sequential steps to refine temporal granularity, thereby obtaining an decomposed MDP formulation. We decompose  $u$  as:

$$u = (u_0, u_1, \dots, u_{T_{seq}}),$$

where  $u_t \in \mathbb{R}^{n_u}$  represents the utilization at time step  $t$ , and  $t \in H = \{1, 2, \dots, T_{seq}\}$  denotes the episodic horizon  $H$ .

Each step  $t$  represents a transport and cargo type, as tuple  $(pol_t, pod_t, k_t)$ . Algorithm 2 illustrates an episode of the decomposed MDP. First, we reset the state  $s_0$ , initialize time  $t$ , and an empty trajectory. The episode iterates over load ports  $(pol_t)$ , discharge ports  $(pod_t)$ , and cargo classes  $(k_t)$ . At each step, we sample action  $x_t$  from policy  $\pi_\theta(x|s_t)$  conditioned on state  $s_t$  and episode parameters  $\zeta$ , and transition to state  $s_{t+1}$ . Afterwards, we store the results in the trajectory and increment time  $t$ . This process continues until all combinations of  $pol_t$ ,  $pod_t$ , and  $k_t$  are explored, accumulating a total of  $T_{seq}$  steps.

#### Transitions.

We use a stochastic transition function  $\mathcal{T}(s_{t+1}|s_t, x_t, \zeta) \in \Delta(S)$ . The transition consists of sequential steps:

1. If  $t \in T_{\text{new port}}$ , port demand is revealed. This means we show  $q_t^{(i,j,k)} \forall (i, j) \in TR_{pol_t}^+, k \in K$ .
2. If  $t \in T_{\text{new port}}$ , onboard cargo is discharged  $u_{t+1} = u_t \odot (1 - \mathbf{e}_t^-)$ , where  $\mathbf{e}_t^- \in \{0, 1\}^{n_q}$  is a binary mask indicating the cargo type and transport to nullify in  $u_t$ .
3. Each time  $t$ , cargo is loaded onboard  $u_{t+1} = u_t + x_t \odot \mathbf{e}_t^+$ , where  $\mathbf{e}_t^+ \in \{0, 1\}^{n_q}$  is a binary indicator specifying cargo types and transports to add to  $u_t$ .

---

**Algorithm 2** Episode of Augmented MDP
 

---

**Require:**  $\mathcal{T}, \pi_\theta, \zeta, \mathcal{Q}$

```

1:  $q_{T_{seq}}^{(i,j,k)} \sim \mathcal{Q}(\mu^{(i,j,k)}, \sigma^{(i,j,k)}) \forall (i,j) \in TR, k \in K$ 
2:  $s_0 \leftarrow (\mathbf{0}^{n_u}, q_{T_{seq}} \odot \mathbf{e}_0^+)$ ,  $t \leftarrow 0$ , Trajectory  $\leftarrow \{\}$ 
3: for  $pol_t = 1$  to  $N_P - 1$  do
4:   for  $pod_t = pol_t + 1$  to  $N_P$  do
5:     for  $k_t \in K$  do
6:        $x_t \sim \pi_\theta(x|s_t, \zeta)$ 
7:        $s_{t+1} \sim \mathcal{T}(s_t, x_t, \zeta)$ 
8:       Append  $(s_t, x_t, r_t, s_{t+1})$  to Trajectory
9:        $t \leftarrow t + 1$ 
10:    end for
11:  end for
12: end for
13: return Trajectory
  
```

---

Additionally, we define the set of time steps before we leave for a new port  $p + 1$  is defined as follows:

$$T_{\text{leave port}} = \left\{ t \in H \mid \exists p \in P_1^{N_P-1} \text{ such that } t = |K| \left( p(N_P - 1) - \frac{p(p-1)}{2} \right) - 1 \right\}.$$

Finally, the set of time steps at which we arrive at a new port  $p$  is defined as follows:

$$T_{\text{new port}} = \left\{ t \in H \mid \exists p \in P_1^{N_P-1} \text{ such that } t = |K| \left( (p-1)(N_P - 1) - \frac{p(p-1)}{2} \right) \right\}.$$

### Feasible Region

The state-dependent feasible region for each time  $t$  is formulated as:

$$PH(s_t) = \{u_t \in \mathbb{R}_{\geq 0}^{n_u} \mid A' u_t \leq b'\}$$

Similar to the port utilization, utilization can be decomposed into load operations and pre-load utilization:

$$u_t = u'_t + u_t^+$$

where:

- $u_t^+ \in \mathbb{R}_{\geq 0}^{n_u}$  represents load operations,
- $u'_t = u_{t-1} - u_t^-$  is the utilization before load operations,
- $u_{t-1} \in \mathbb{R}_{\geq 0}^{n_u}$  is the previous step's utilization,
- $u_t^- \in \mathbb{R}_{\geq 0}^{n_u}$  is the discharge operations.

Using the decomposition, we obtain the feasible region as:

$$PH(s_t) = \{u_t \in \mathbb{R}_{\geq 0}^{n_u} \mid A'(u_t^+ + u'_t) \leq b'\}$$

### Substituting Load Operations for Actions

Actions  $x_t$  correspond to transformed load operations  $u_t^+$ , given by:

$$x_t = u_t^+ M(s_t), \quad M(s_t) \in \{0, 1\}^{n_u \times n_c},$$

where  $M(s_t)$  is a state-dependent sparsity mask that selects relevant elements from  $u_t^+$ .

However, load operations are subject to  $m_u$  constraints, whereas actions adhere to  $m_c$  constraints. To bridge this difference, we define the state-dependent constraint matrix:

$$A(s_t) = T(s_t)^\top A' M(s_t), \quad T(s_t) \in \{0, 1\}^{m_u \times m_c},$$

where:

- $A'$  is the original constraint matrix of shape  $(m_u, n_u)$ ,
- $T(s_t)$  maps the constraints of  $u_t^+$  to that of  $x_t$
- $M(s_t)$  maps the space of  $u_t^+$  to that of  $x_t$ ,

Similarly, we introduce a state-dependent bound:

$$b''(s_t) = T(s_t)^\top b',$$

where:

- $b'$  is the original bound of shape  $(m_u, 1)$ ,
- $T(s_t)$  maps the constraints of  $u_t^+$  to that of  $x_t$

### Feasible Region for Actions

Using the refined notation, we express the state-dependent feasible region in terms of actions:

$$PH(s_t) = \{x_t \in \mathbb{R}_{\geq 0}^{n_c} \mid A(s_t)x_t \leq b''(s_t) - A'u'_t\}.$$

Next, we define the updated bound as:

$$b(s_t) = b''(s_t) - A'u'_t.$$

Substituting this into the feasible region, we obtain:

$$PH(s_t) = \{x_t \in \mathbb{R}_{\geq 0}^{n_c} \mid A(s_t)x_t \leq b(s_t)\}.$$

### A.4 MPP Constraints

Let us specify the MPP constraints of  $PH(s_p)$  and  $PH(s_t)$ .

#### Demand Constraints

Let us consider the demand subset of  $PH(s_p)$  as:

$$PH(s_p)_{\text{dem}} = \{x_p \in \mathbb{R}_{\geq 0}^{n_u} \mid A'_{\text{dem}} x_p \leq b'_{\text{dem}} - A'_{\text{dem}} u'_p\}.$$

We sum over all vessel locations to obtain an aggregated number of containers of shape  $n_q$ . Note that only current load actions  $x_p$  are relevant for  $q_p$ , hence we can omit  $A'_{\text{dem}} u'_p$  as pre-loading utilization has already satisfied its demand requirements.

$$x_p^\top \mathbf{1}_{n_c} \leq q_p$$

Consider the demand subset of  $PH(s_t)$  as:

$$PH(s_t)_{\text{dem}} = \{x_t \in \mathbb{R}_{\geq 0}^{n_c} \mid A(s_t)_{\text{dem}} x_t \leq b'(s_t)_{\text{dem}} - A'_{\text{dem}} u'_t\}.$$

Right now, we can sum the full vector  $x_t$  as it needs to sum to scalar  $q_t^{(pol_t, pod_t, k_t)}$ . Again, previous steps are irrelevant to demand, hence we can disregard  $A'_{\text{dem}} u'_t$  to obtain:

$$\mathbf{1}^\top x_t \leq q_t^{(pol_t, pod_t, k_t)}$$

### Capacity Constraints

Let us consider the constraint subset of  $PH(s_p)$  as:

$$PH(s_p)_{\text{cap}} = \{x_p \in \mathbb{R}_{\geq 0}^{n_u} \mid A'_{\text{cap}} x_p \leq b'_{\text{cap}} - A'_{\text{cap}} u'_p\}.$$

We sum TEU of all cargo types and transports in  $x_p$  to obtain TEU use per location with shape  $n_c$ . The TEU of pre-load utilization is also considered by subtracting it from the vessel capacity, obtaining the following:

$$x_p \text{teu} \leq c - u'_p \text{teu},$$

Consider the demand subset of  $PH(s_t)$  as:

$$PH(s_t)_{\text{cap}} = \{x_t \in \mathbb{R}_{\geq 0}^{n_c} \mid A(s_t)_{\text{cap}} x_t \leq b'(s_t)_{\text{cap}} - A'_{\text{cap}} u'_t\}.$$

Now, we can do the same trick based on a single scalar  $\text{teu}^{(pol_t, pod_t, k_t)}$  multiplied with the sum of action  $x_t$ .

$$\text{teu}^{(pol_t, pod_t, k_t)} \mathbf{1}^\top x_t \leq c - u'_t \text{teu},$$

### Stability Constraints

The stability constraints require some algebra to derive for  $PH(s_p)$  and  $PH(s_t)$ .

The lcg constraint in its original form is given by:

$$\frac{\mathbf{1}^\top (lm \odot u_p)}{\mathbf{1}^\top (w \odot u_p)} \leq \overline{lcg}.$$

Applying the utilization decomposition, we can obtain the formulation for  $PH(s_p)$ :

$$\begin{aligned} \mathbf{1}^\top (lm \odot u_p) &\leq \overline{lcg} \mathbf{1}^\top (w \odot u_p) \\ \mathbf{1}^\top (lm \odot u_p^+) + \mathbf{1}^\top (lm \odot u'_p) &\leq \overline{lcg} \mathbf{1}^\top (w \odot u_p^+) \\ &\quad + \overline{lcg} \mathbf{1}^\top (w \odot u'_p) \\ \mathbf{1}^\top (lm_p \odot x_p) - \overline{lcg} \mathbf{1}^\top (w \odot x_p) &\leq \overline{lcg} \mathbf{1}^\top (w \odot u'_p) \\ &\quad - \mathbf{1}^\top (lm \odot u'_p) \\ \mathbf{1}^\top ((lm - \overline{lcg} w) \odot x_p) &\leq \mathbf{1}^\top ((\overline{lcg} w - lm) \odot u'_p). \end{aligned}$$

This approach extends to both the lower and upper bounds for the lcg and vcg, ensuring that vessel stability is properly maintained at every step.

Based on the  $PH(s_p)$  constraint, we can substitute load operations for actions, and obtain the formulation for  $PH(s_t)$ :

$$\mathbf{1}^\top ((lm(t) - \overline{lcg} w(t)) \odot x_t) \leq \mathbf{1}^\top ((\overline{lcg} w - lm) \odot u'_p).$$

where  $w(t) = w^{(pol_t, pod_t, k_t)}$  and  $lm(t) = lm^{(pol_t, pod_t, k_t)}$

### A.5 Auxiliary Variables

The reward function contains two auxiliary variables derived from state  $s$ , which incur costs due to inefficient port operations. At port  $p$ , Equation (14) creates an indicator of hatch movements  $hm(s, p) \in \{0, 1\}^{|B|}$ , whereas Equation (15) computes the number of on-deck containers during hatch movements, causing hatch overstockage  $ho(s, p) \in \mathbb{R}_{\geq 0}^{|B|}$ .

$$hm(s, p) = \left( \sum_{k \in K} \sum_{tr \in TR_p^M} u_t^{(b, d^{below}, k, tr)} > 0 \right) \quad (14)$$

$$ho(s, p) = hm(s, p) \left( \sum_{k \in K} \sum_{tr \in TR_p^{AC}} u_t^{(b, d^{above}, k, tr)} \right) \quad (15)$$

Equation (16) computes the target crane moves at port  $p$  by equally spreading the total demand per port over pairs of adjacent bays, where  $\delta^{cm}$  is the allowed deviation from the equal spread set by ports. Subsequently, Equation (17) computes the excess crane moves  $cm(s, p) \in \mathbb{R}_{\geq 0}^{|B|-1}$

$$\overline{cm}(s, p) = (1 + \delta^{cm}) \frac{2}{|B|} \sum_{tr \in TR_p^M} \sum_{k \in K} q_t^{(tr, k)} \quad (16)$$

$$\begin{aligned} cm(s, p) = \max \left( \overline{cm}(s, p) - \sum_{d \in D} \sum_{k \in K} \sum_{tr \in TR_p^M} u_t^{(0:|B|-1, d, k, tr)} \right. \\ \left. + u_t^{(1:|B|, d, k, tr)}, 0 \right) \quad (17) \end{aligned}$$

## B Feasibility Mechanisms

Table 2 provides an overview of implemented feasibility mechanisms.

Type	Implementation	Constraints
FR	Composite loss	Constraints $PH(s_t)$
VP	$VP(x_t, A(s_t), b(s_t), \alpha_v, \delta_v)$	Constraints $PH(s_t)$
WS	$\mathcal{W}(x_t, q_t)$	Demand $q_t$
PC	$\mathcal{C}(x_t, 0, c - u'_t \text{teu})$	TEU capacity $c$

Table 2: Feasibility mechanisms and relation to constraints

### B.1 Log Probability Adjustments

This subsection provides technical details on the adjustments made to the log-probability distribution of the policy as a result of non-linear transformations to distribution samples.

Projecting actions alters the policy's probability density, necessitating consideration of the change of variables principle [Bishop, 2006]. This principle ensures valid volume scaling by requiring the transformation  $f(x)$  to satisfy:

1. **Differentiability:**  $f(x)$  must be differentiable to compute the Jacobian  $J_f(x)$  and determine local volume scaling.
2. **Non-Singularity:** The Jacobian determinant must be non-zero ( $\det(J_f(x)) \neq 0$ ) to prevent dimensional collapse.
3. **Invertibility:**  $f(x)$  must be locally or globally invertible to ensure a one-to-one mapping between points in the original and transformed spaces.

These properties ensure the transformation is smooth, one-to-one, and well-behaved, enabling the use of the Jacobian adjustment  $\log \pi'(x|s) = \log \pi(x|s) - \log |\det(J_f(x))|$  as a valid probability scaling factor.

### Weighted Scaling Projection Layer.

Suppose we have variable  $x \in \mathbb{R}_{>0}^n$  and scalar  $y \in \mathbb{R}_{>0}$  and the following piecewise linear function:

$$\mathcal{P}(x, y) = \begin{cases} x & \text{if } \mathbf{1}^\top x \leq y \\ \frac{x}{\mathbf{1}^\top x} \cdot y & \text{if } \mathbf{1}^\top x > y \end{cases}$$

Case 1:  $\mathbf{1}^\top x \leq y$ .

$$\begin{aligned} \mathcal{P}(x, y) &= x \\ \frac{\partial}{\partial x} \mathcal{P}(x, y) &= \frac{\partial x}{\partial x} \\ J_{\mathcal{P}}(x, y) &= I_n \end{aligned}$$

Case 2:  $\mathbf{1}^\top x > y$ , where we apply the product rule and then the quotient rule of differentiation.

$$\begin{aligned} \mathcal{P}(x, y) &= \frac{x}{\mathbf{1}^\top x} \cdot y \\ \frac{\partial}{\partial x} \mathcal{P}(x, y) &= \frac{\partial}{\partial x} \left( \frac{x}{\mathbf{1}^\top x} \cdot y \right) \\ \frac{\partial}{\partial x} \mathcal{P}(x, y) &= \frac{\partial}{\partial x} \left( \frac{x}{\mathbf{1}^\top x} \right) \cdot y \\ J_{\mathcal{P}}(x, y) &= y \cdot \frac{1}{(\mathbf{1}^\top x)^2} (I_n \mathbf{1}^\top x - x \cdot \mathbf{1}^\top) \\ J_{\mathcal{P}}(x, y) &= \frac{y \cdot I_n}{(\mathbf{1}^\top x)} - \frac{y \cdot x^\top}{(\mathbf{1}^\top x)^2} \end{aligned}$$

We obtain the following Jacobian of function  $\mathcal{P}(x, y)$ :

$$J_{\mathcal{P}}(x, y) = \begin{cases} I_n & \text{if } \mathbf{1}^\top x \leq y \\ \frac{y}{(\mathbf{1}^\top x)^2} (I_n \mathbf{1}^\top x - x \mathbf{1}^\top) & \text{if } \mathbf{1}^\top x > y \end{cases}$$

Finally, we verify that Jacobian adjustment is allowed for the weighted scaling projection by:

1.  $\mathcal{P}(x, y)$  has been shown to be differentiable.
2. Provided that  $x, y > 0$ , either case is positive definite as the diagonal elements are strictly positive. We obtain  $\det(J_{\mathcal{P}}(x, y)) > 0$ , thus the Jacobian is non-singular.
3.  $\mathcal{P}(x, y)$  is locally invertible as  $\det(J_{\mathcal{P}}(x, y)) \neq 0$ .

### Violation Projection Layer.

Suppose we have function  $\mathcal{P}(x, A, b) = x - \eta_v A^\top (Ax - b)_{>0}$  with  $x \in \mathbb{R}_{>0}^n$ ,  $\eta_v \in \mathbb{R}_{>0}$ ,  $A \in \mathbb{R}_{\geq 0}^{m \times n}$ ,  $b \in \mathbb{R}_{\geq 0}^m$ , and  $m > n$ .

Case 1:  $\eta_v A^\top (Ax - b) = 0$ .

$$\begin{aligned} \mathcal{P}(x, A, b) &= x \\ \frac{\partial}{\partial x} \mathcal{P}(x, A, b) &= \frac{\partial x}{\partial x} \\ J_{\mathcal{P}}(x, A, b) &= I_n \end{aligned}$$

Case 2:  $\eta_v A^\top (Ax - b) > 0$ , where we apply the chain rule on the second term.

$$\mathcal{P}(x, A, b) = x - \eta_v A^\top (Ax - b)$$

$$\begin{aligned} \frac{\partial}{\partial x} \mathcal{P}(x, A, b) &= \frac{\partial}{\partial x} (x - \eta_v A^\top (Ax - b)) \\ J_{\mathcal{P}}(x, A, b) &= I_n - \eta_v A^\top A \end{aligned}$$

Both cases are combined in the following matrix formulation with diagonal matrix  $\text{Diag} = \text{diag}((Ax - b) > 0)$ :

$$J_{\mathcal{P}}(x, A, b) = I_n - \eta_v A^\top \text{Diag} A$$

Finally, we can confirm that Jacobian adjustment is allowed for the violation projection layer by:

1.  $\mathcal{P}(x, A, b)$  is differentiable as shown above.
2. Due to the full rank nature of the identity  $I_n$  and  $A^\top \text{Diag} A$  when  $\text{Diag} = I_m$ , we get  $\det(J_{\mathcal{P}}(x, A, b)) \neq 0$ , and hence the Jacobian is non-singular.
3.  $\mathcal{P}(x, A, b)$  is locally invertible as  $\det(J_{\mathcal{P}}(x, A, b)) \neq 0$ . It is not globally invertible, due to the piece-wise nature of  $(Ax - b)_{>0}$ .

### Policy Clipping

We can implement a clipped Gaussian distribution that enforces element-wise bounds on a standard Gaussian [Fujita and Maeda, 2018]. Let  $\mu_\theta$  and  $\sigma_\theta^2$  denote the policy's mean and variance, with bounds  $lb_{pc}$  and  $ub_{pc}$ , and  $\Phi(\cdot)$  being the cumulative distribution function of the standard Gaussian. Actions are sampled from  $\mathcal{N}(\mu_\theta, \sigma_\theta^2)$  and clipping the result to  $[lb_{pc}, ub_{pc}]$ . Provided this transformation, we compute the log probabilities  $\log \pi(x|s)$  for action  $x$  by:

$$\log \pi(x|s) = \begin{cases} \log \Phi \left( \frac{lb_{pc} - \mu_\theta}{\sigma_\theta} \right) & \text{if } x \leq lb_{pc}, \\ -\frac{(x - \mu_\theta)^2}{2\sigma_\theta^2} - \log(\sqrt{2\pi\sigma_\theta^2}) & \text{if } lb_{pc} < x < ub_{pc}, \\ \log \left( 1 - \Phi \left( \frac{ub_{pc} - \mu_\theta}{\sigma_\theta} \right) \right) & \text{if } x \geq ub_{pc} \end{cases}$$

### B.2 Violation Projection Layer

We define a feasible region of action  $x$  as the polyhedron:

$$PH = \{x \in \mathbb{R}^n : Ax \leq b, x \geq 0\},$$

where  $A \in \mathbb{R}^{m \times n}$  and  $b \in \mathbb{R}^m$ .

Constraints in  $PH$  may be violated during optimization. To quantify these violations, we introduce the violation function:

$$\mathcal{V}(x) = (Ax - b)_{>0},$$

where  $\mathcal{V}(x)_{m_i} > 0$  indicates that constraint  $m_i$  is violated, and  $\mathcal{V}(x)_{m_i} = 0$  means the constraint is satisfied.

**Violation Gradient Descent.** To minimize constraint violations, we update  $x$  for a fixed number of iterations using gradient descent on the violation term  $\|\mathcal{V}(x)\|_2^2$ , which represents the squared distance to feasibility. Differentiating with respect to  $x$ , we derive the update rule:

$$\begin{aligned} x' &= x - \eta_v \nabla_x \|\mathcal{V}(x)\|_2^2 \\ &= x - \eta_v 2A^\top \mathcal{V}(x). \end{aligned}$$

Since the step size  $\eta_v \in (0, 1)$  is a tunable parameter, we simplify the update function to:

$$x' = x - \eta_v A^\top \mathcal{V}(x).$$

**Theorem 1** (Convergence of Violation Gradient Descent). *Let  $x_0 \in \mathbb{R}^n$  be an initial point, and consider update:*

$$x_{k+1} = x_k - \eta_v A^\top \mathcal{V}(x_k),$$

where:

- $\mathcal{V}(x) = \max(0, Ax - b)$  is the element-wise function onto nonnegative constraint values.
- $\eta_v \in (0, 1)$  is a step size parameter.
- $A \in \mathbb{R}^{m \times n}$  has full row rank.
- The feasible region  $PH = \{x \in \mathbb{R}^n : Ax \leq b, x \geq 0\}$  is nonempty.

Then, the sequence  $\{x_k\}$  satisfies:

1. The function  $g(x) = \|\mathcal{V}(x)\|_2^2$  is non-increasing.
2.  $x_k$  converges to a feasible point  $x^*$  or a local minimum violation point.

*Proof.* Define the violation function:

$$g(x) = \|\mathcal{V}(x)\|_2^2.$$

Since  $\mathcal{V}(x)$  is an elementwise projection onto nonnegative values, and some function  $h(y) = \max(0, y)$  is convex and non-decreasing, then the function  $g(x) = \|\mathcal{V}(x)\|_2^2$  is convex when  $Ax - b$  is affine.

We apply gradient descent on  $g(x)$  using the update rule:

$$x_{k+1} = x_k - \eta_v \nabla_x g(x_k).$$

By the standard descent lemma [Boyd and Vandenberghe, 2004], for a sufficiently small step size  $\eta_v$ , we have:

$$g(x_{k+1}) \leq g(x_k) - \eta_v \|\nabla_x g(x_k)\|_2^2.$$

Since  $\eta_v > 0$  and  $\|\nabla_x g(x_k)\|_2^2 \geq 0$ , it follows that:

$$g(x_{k+1}) \leq g(x_k).$$

Thus,  $g(x_k)$  is non-increasing.

Since  $g(x_k)$  is also lower-bounded by 0, it must converge to some limit  $g^* \geq 0$ . This implies:

$$\lim_{k \rightarrow \infty} \|\mathcal{V}(x_k)\|_2 = \tilde{c}, \quad \text{for some } \tilde{c} \geq 0.$$

If  $\tilde{c} = 0$ , then  $x_k$  converges to a feasible point, meaning  $\mathcal{V}(x_k) = 0$ . If  $\tilde{c} > 0$ , then  $x_k$  converges to a local minimum of  $g(x)$ , where no further descent is possible, satisfying  $\nabla_x g(x_k) = 0$ , which implies  $A^\top \mathcal{V}(x_k) = 0$ .  $\square$

## C Instance Generator

During training, we simulate problem instances based on a Gaussian distribution with element  $i$ :

$$q^{(i,j,k)} \sim \mathcal{N}(\mu^{(i,j,k)}, \sigma^{(i,j,k)}) \quad \forall (i,j) \in TR, k \in K.$$

Here,  $\mu$  is the expected value of cargo demand, initialized by a uniform generator  $\mathcal{U}(lb, ub)$ , while the standard deviation of demand is defined as  $\sigma^{(i,j,k)} = CV \cdot \mu^{(i,j,k)}$ , where the coefficient of variation (CV) controls the spread of each element based on  $\mu^{(i,j,k)}$ . Note that CV is normally defined

as  $CV^{(i,j,k)} = \frac{\sigma^{(i,j,k)}}{\mu^{(i,j,k)}}$ , so we use  $\sigma^{(i,j,k)} = CV \cdot \mu^{(i,j,k)}$  to control the spread of the distribution.

We initialize  $\mu^{(i,j,k)} \sim \mathcal{U}(0, \overline{\mu^{(i,j,k)}})$ , where the upper bound on the expected value is found as follows:

$$\bar{\mu} = \frac{2UR \cdot \mathbf{1}^\top c}{NC},$$

where  $UR$  is the rate of total utilization present in the demand (e.g., 1.2 means total demand is 120% of total capacity), and  $NC \in \mathbb{R}_{>0}^{|TR|}$  is a matrix to spread the demand over different elements proportional to the number of transports remaining to be loaded.

During generalization testing, we simulate problem instances based on a continuous uniform generator:

$$q^{(i,j,k)} \sim \mathcal{U}(lb^{(i,j,k)}, ub^{(i,j,k)}).$$

To ensure similar mean and variance of the instances, we derive parameters  $a$  and  $b$  from the definition of the continuous uniform distribution, as follows:

$$\begin{aligned} \mu^{(i,j,k)} &= (lb^{(i,j,k)} + ub^{(i,j,k)})/2 \\ (\sigma^{(i,j,k)})^2 &= (ub^{(i,j,k)} - lb^{(i,j,k)})^2/12 \end{aligned}$$

We rewrite to:

$$\begin{aligned} lb^{(i,j,k)} &= \mu^{(i,j,k)} - \sqrt{(12(\sigma^{(i,j,k)})^2)/2} \\ ub^{(i,j,k)} &= \mu^{(i,j,k)} + \sqrt{(12(\sigma^{(i,j,k)})^2)/2} \end{aligned}$$

## D Multi-stage Stochastic MIP

### D.1 Multi-stage Scenario Tree

A scenario tree is a directed tree represented as  $T_{ST} = (V_{ST}, E_{ST})$ , where  $V_{ST}$  is the set of nodes, each corresponding to a decision or uncertainty realization at a given stage.  $E_{ST} \subseteq V_{ST} \times V_{ST}$  is the set of directed edges representing transitions between nodes over time.

The tree consists of:

1. A root node  $v_1 \in V_{ST}$ , representing the initial state at the first port.
2. Stages  $p = 1, 2, \dots, N_P - 1$ , where each node  $v$  belongs to a stage  $p(v)$ . We denote stages by  $p$ , as stages are equivalent to ports in a voyage.
3. Branching structure, where each node has child nodes that correspond to possible future realizations.
4. A probability measure  $P : V_{ST} \rightarrow [0, 1]$  assigning probabilities to nodes, ensuring:

$$\sum_{v' \in \text{child}(v)} \mathbb{P}(v') = \mathbb{P}(v), \quad \forall v \in V_{ST}.$$

5. Scenario paths  $\phi \in \mathcal{Z}$ , which are root-to-leaf paths representing possible realizations of uncertainty over time.



## D.2 MIP Formulation

We define the MPP under demand uncertainty as a multi-stage stochastic MIP.

**Decision Variables.** The following variables are included:

- Vessel utilization:  $\tilde{u}_{tr,k}^{b,d,\phi} \in \mathbb{Z}_{\geq 0}$
- Hatch overstockage:  $\tilde{ho}_{p,b}^{\phi} \in \mathbb{Z}_{\geq 0}$
- Makespan of cranes:  $\tilde{cm}_p^{\phi} \in \mathbb{Z}_{\geq 0}$
- Hatch movement:  $\tilde{hm}_{p,b}^{\phi} \in \{0, 1\}$

In addition, we introduce the big  $M$  as a sufficiently large constant used to enforce logical constraints.

**Objective.** The objective function (18) maximizes the revenue and minimizes hatch-overstockage and crane moves costs over scenario paths  $\phi \in \mathcal{Z}$  each with probability  $\mathbb{P}_{\phi}$ . We assume each scenario path has equal probability.

**Constraints.** Constraint (19) enforces that the onboard utilization cannot exceed the cargo demand  $q$ , whereas Constraint (20) limits each vessel location to the TEU capacity  $c$  for each bay  $b \in B$  and deck  $d \in D$ . In Constraint (21), we indicate that hatches need to be opened if below deck cargo needs to be loaded or discharged. Based on these movements, Constraint (22) models the amount of hatch overstockage in containers. Subsequently, we compute the target of crane moves  $\bar{z}$  in Constraint (23), after which Constraint (24) computes the excess number of crane moves  $\tilde{cm}$ .

Additionally, we model the longitudinal and vertical stability in Constraints (26) until (29). First, we compute the longitudinal moment, vertical moment and total weight in Constraints (26), (27) and (25), respectively. Second, Constraint (28) bounds  $l_{cg}$  between  $\underline{l_{cg}}$  and  $\overline{l_{cg}}$ . Third, Constraint (29) bounds  $v_{cg}$  between  $\underline{v_{cg}}$  and  $\overline{v_{cg}}$ . Both  $l_{cg}$  and  $v_{cg}$  are linearized equivalents of the original Constraints (1) and (2), respectively. Furthermore, we include non-anticipation in Constraint (30) to prevent leveraging future demand realizations.

$$\max \sum_{\phi \in \mathcal{Z}} \mathbb{P}_{\phi} \sum_{p \in P} \sum_{b \in B} \sum_{d \in D} \sum_{k \in K} \sum_{tr \in TR^+(p)} f_1 \tilde{u}_{tr,k}^{b,d,\phi} - f_2 \tilde{ho}_{p,b}^{\phi} - f_3 \tilde{cm}_p^{\phi} \quad (18)$$

$$\text{s.t.} \sum_{b \in B} \sum_{d \in D} \tilde{u}_{tr,k}^{b,d,\phi} \leq q_{tr,k}^{\phi} \quad \forall p \in P, tr \in TR^{OB}(p), k \in K, \phi \in \mathcal{Z} \quad (19)$$

$$\sum_{k \in K} \sum_{tr \in TR^{OB}(p)} te_{tr,k} \tilde{u}_{tr,k}^{b,d,\phi} \leq c_{b,d} \quad \forall p \in P, b \in B, d \in D, \phi \in \mathcal{Z} \quad (20)$$

$$\sum_{k \in K} \sum_{tr \in TR^M(p)} \tilde{u}_{tr,k}^{b,d,\phi} \leq M \tilde{hm}_{p,b}^{\phi} \quad \forall p \in P, b \in B, \phi \in \mathcal{Z} \quad (21)$$

$$\sum_{k \in K} \sum_{tr \in TR^{AC}(p)} \tilde{u}_{tr,k}^{b,d,\phi} - M(1 - \tilde{hm}_{p,b}^{\phi}) \leq \tilde{ho}_{p,b}^{\phi} \quad \forall p \in P, b \in B, \phi \in \mathcal{Z} \quad (22)$$

$$\bar{z}_p^{\phi} = (1 + \delta^{cm}) \frac{2}{|B|} \sum_{tr \in TR^M(p)} \sum_{k \in K} q_{tr,k}^{\phi} \quad \forall p \in P, \phi \in \mathcal{Z} \quad (23)$$

$$\bar{z}_p^{\phi} - \sum_{b \in B'} \sum_{d \in D} \sum_{k \in K} \sum_{tr \in TR^M(p)} \tilde{u}_{tr,k}^{b,d,\phi} \leq \tilde{cm}_p^{\phi} \quad \forall p \in P, b' \in B', \phi \in \mathcal{Z} \quad (24)$$

$$tw_p^{\phi} = \sum_{k \in K} w_k \sum_{tr \in TR^{OB}(p)} \sum_{d \in D} \sum_{b \in B} \tilde{u}_{tr,k}^{b,d,\phi} \quad \forall p \in P, \phi \in \mathcal{Z} \quad (25)$$

$$lm_p^{\phi} = \sum_{b \in B} ld_b \sum_{k \in K} w_k \sum_{tr \in TR^{OB}(p)} \sum_{d \in D} \tilde{u}_{tr,k}^{b,d,\phi} \quad \forall p \in P, \phi \in \mathcal{Z} \quad (26)$$

$$vm_p^{\phi} = \sum_{d \in D} vd_d \sum_{k \in K} w_k \sum_{tr \in TR^{OB}(p)} \sum_{b \in B} \tilde{u}_{tr,k}^{b,d,\phi} \quad \forall p \in P, \phi \in \mathcal{Z} \quad (27)$$

$$\underline{l_{cg}tw}_p^{\phi} \leq lm_p^{\phi} \leq \overline{l_{cg}tw}_p^{\phi} \quad \forall p \in P, \phi \in \mathcal{Z} \quad (28)$$

$$\underline{v_{cg}tw}_p^{\phi} \leq vm_p^{\phi} \leq \overline{v_{cg}tw}_p^{\phi} \quad \forall p \in P, \phi \in \mathcal{Z} \quad (29)$$

$$\tilde{u}_{tr,k}^{b,d,\phi'} = \tilde{u}_{tr,k}^{b,d,\phi} \quad \forall p \in P, tr \in TR^+(p), k \in K, b \in B, d \in D, \phi, \phi' \in \mathcal{Z} \mid q_{[p-1]}^{\phi} = q_{[p-1]}^{\phi'} \quad (30)$$

## E Deep RL Implementation Details

To prevent confusion, we

### E.1 PPO Algorithm

PPO is an on-policy reinforcement learning algorithm that seeks to maximize expected cumulative reward while enforcing stable policy updates via clipped importance sampling [Schulman *et al.*, 2017], as outlined in Algorithm 3. The agent collects trajectories, computing  $n_{ppo}$ -step return to evaluate performance with  $V_{\theta}(s)$  as estimated state value:

$$G_t^{(n_{ppo})} = \sum_{k_{ppo}=0}^{n_{ppo}-1} \gamma^k r_{t+k_{ppo}} + \gamma^{n_{ppo}} V_{\theta}(s_{t+n_{ppo}}), \quad (31)$$

To reduce variance, we adopt Generalized Advantage Estimation (GAE) [Schulman *et al.*, 2016]:

$$\hat{A}_t^{GAE} = \sum_{l_{ppo}=0}^{\infty} (\gamma \lambda)^{l_{ppo}} \delta_{t+l_{ppo}}, \quad (32)$$

$$\delta_t = r_t + \gamma V_{\theta}(s_{t+1}) - V_{\theta}(s_t). \quad (33)$$

Here,  $\delta_t$  is the temporal difference (TD) residual, which quantifies the advantage of taking action  $x_t$  at state  $s_t$ .

The actor is updated using the PPO clipped surrogate loss:

$$\mathcal{L}_{actor}(\theta) = \mathbb{E}_t \left[ \min \left( \text{ratio}_t(\theta) \hat{A}_t^{GAE}, \right. \right.$$

$$\text{clip}(\text{ratio}_t(\theta), 1 - \epsilon, 1 + \epsilon) \hat{A}_t^{\text{GAE}}], \quad (34)$$

where the probability ratio is defined as:

$$\text{ratio}_t(\theta) = \frac{\pi_\theta(x_t | s_t)}{\pi_{\theta_{\text{old}}}(x_t | s_t)}. \quad (35)$$

The critic aims to minimize the squared TD error:

$$\mathcal{L}_{\text{critic}}(\theta) = \mathbb{E}_t \left[ (V_\theta(s_t) - G_t^{(n_{\text{ppo}})})^2 \right]. \quad (36)$$

Finally, the total PPO objective, including feasibility regularization from Equation (11), is given by:

$$\begin{aligned} \mathcal{L}(\theta) = & \mathcal{L}_{\text{actor}}(\theta) + \lambda_c \mathcal{L}_{\text{critic}}(\theta) + \lambda_f \mathcal{L}_{\text{feas}}(\theta) \\ & - \lambda_e \mathbb{E}_t [\text{entropy}(\pi_\theta)], \end{aligned} \quad (37)$$

where  $\lambda_c$ ,  $\lambda_f$ , and  $\lambda_e$  are weighting coefficients for the critic loss, feasibility regularization, and entropy regularization respectively.

---

### Algorithm 3 Proximal Policy Optimization (PPO)

---

**Require:** Model parameters  $\theta$ , steps  $n$ , learning rate  $\eta$

- 1: **for** each gradient update **do**
  - 2:   **for** each step  $t$  **do**
  - 3:     Collect  $n$ -step trajectories  $\{(s_t, x_t, r_t, s_{t+1})\}$
  - 4:     Compute  $n$ -step returns  $G_t^{(n_{\text{ppo}})}$
  - 5:     Compute advantage estimates  $\hat{A}_t^{\text{GAE}}$
  - 6:   **end for**
  - 7:   Update parameters:  $\theta \leftarrow \theta + \eta \nabla_\theta \mathcal{L}(\theta)$
  - 8: **end for**
  - 9: **return** Policy  $\pi_\theta$
- 

## E.2 SAC Algorithm

Soft Actor-Critic (SAC) is an off-policy reinforcement learning algorithm that optimizes both reward maximization and entropy to encourage efficient exploration [Haarnoja *et al.*, 2018], as outlined in Algorithm 4. It is based on maximum entropy reinforcement learning, which aims to learn a stochastic policy that not only maximizes cumulative rewards but also maintains high entropy for robustness and stability. SAC leverages a soft Q-learning approach, using two Q-functions to mitigate overestimation bias, an entropy-regularized policy update, and an automatically adjusted temperature parameter to balance exploration and exploitation.

The algorithm maintains an actor network for policy learning, two Q-function critics for value estimation, a target Q-network for stable learning, and an adaptive temperature parameter to regulate entropy. The loss functions for standard SAC are derived from the Bellman backup equation and the policy gradient formulation, ensuring convergence to an optimal stochastic policy. We also include feasibility regularization from Equation (11) in the actor loss.

- Compute target Q-value:

$$Q_{\text{target}}(s_t, x_t) = r_t + \gamma \mathbb{E}_{s_{t+1}, x_{t+1} \sim \pi} \left[ \min_{l=1,2} Q_\theta^l(s_{t+1}, x_{t+1}) - \alpha \log \pi_\theta(x_{t+1} | s_{t+1}) \right]$$

- Critic loss:

$$\mathcal{L}_{\text{critic}}(\theta) = \mathbb{E} \left[ (Q_\theta(s_t, x_t) - Q_{\text{target}}(s_t, x_t))^2 \right]$$

- Actor loss:

$$\mathcal{L}_{\text{actor}}(\theta) = \mathbb{E} \left[ \alpha \log \pi_\theta(x_t | s_t) - Q_\theta(s_t, x_t) + \lambda_f \mathcal{L}_{\text{feas}}(\theta) \right]$$

- Temperature loss:

$$\mathcal{L}_\alpha(\theta) = \mathbb{E} \left[ -\alpha (\log \pi_\theta(x_t | s_t) + \text{entropy}_{\text{target}}) \right]$$

This formulation ensures stability and encourages exploration by adapting the trade-off between exploitation and exploration dynamically.

---

### Algorithm 4 Soft Actor-Critic (SAC)

---

**Require:** Parameters: actor  $\theta_{\text{actor}}$ , critics  $\theta_{\text{critic}}^1, \theta_{\text{critic}}^2$ , targets  $(\theta_{\text{target}}^1, \theta_{\text{target}}^2) = (\theta_{\text{critic}}^1, \theta_{\text{critic}}^2)$ , temperature  $\alpha$ , learning rate actor  $\eta_a$ , learning rate critic  $\eta_c$ , learning rate temperature  $\eta_\alpha$ , soft update parameter  $\tau$ , replay buffer  $\mathcal{D}$ .

- 1: **for** each step  $t$  **do**
  - 2:   Sample action  $x_t \sim \pi_\theta(x_t | s_t)$
  - 3:   Perform transition  $s_{t+1} \sim \mathcal{T}(s_{t+1} | s_t, x_t)$
  - 4:   Observe reward  $r_t = \mathcal{R}(s_t, x_t)$ ,
  - 5:   Store  $(s_t, x_t, r_t, s_{t+1})$  in  $\mathcal{D}$ .
  - 6: **end for**
  - 7: **for** each gradient update **do**
  - 8:   Sample a minibatch  $(s_t, x_t, r_t, s_{t+1})$  from  $\mathcal{D}$ .
  - 9:   Compute target Q-value:  $Q_{\text{target}}(s_t, x_t)$
  - 10:   Update parameters:
 
$$\begin{aligned} \theta_{\text{critic}}^l & \leftarrow \theta_{\text{critic}}^l - \eta_c \nabla_l \mathcal{L}_{\text{critic}}(\theta) \text{ for } l \in \{1, 2\} \\ \theta_{\text{actor}} & \leftarrow \theta_{\text{actor}} - \eta_a \nabla \mathcal{L}_{\text{actor}}(\theta) \\ \alpha & \leftarrow \alpha - \eta_\alpha \nabla \mathcal{L}_\alpha(\theta) \\ \theta_{\text{target}}^l & \leftarrow \tau \theta_{\text{critic}}^l + (1 - \tau) \theta_{\text{target}}^l \text{ for } l \in \{1, 2\} \end{aligned}$$
  - 11: **end for**
- 

## E.3 Hyperparameters

Parameters of the MPP environment are shown in Table 3.

Table 4 provides the hyperparameters of projected and vanilla PPO and SAC.

## E.4 Additional Experiments

In Table 5, we analyze different configurations of feasibility regularization (FR). First, we evaluate performance under the same hyperparameters as AM-P policies. Second, we examine the effect of significantly increasing  $\lambda_f$ . Third, we assess performance with specific hyperparameter tuning, including  $\lambda_f$ . These experiments indicate that FR can reduce the distance to the feasible region, however, achieving fully feasible instances remains a challenge.

Parameters	Symbol	Value
Voyage length	$N_P$	4
Number of bays	$N_B$	10
Cardinality deck set	$ D $	2
Cardinality cargo set	$ K $	12
Cardinality transport set	$ TR $	6
Vessel TEU	$\mathbf{1}^\top c$	1,000
Long term contract reduction	$LR$	0.3
Utilization rate demand	$UR$	1.1
lcg bounds	$(lcg, \overline{lcg})$	(0.85,1.05)
vcg bounds	$(vcg, \overline{vcg})$	(0.95,1.15)
Crane moves allowance	$\delta^{cm}$	0.25
Overstowage costs	$ct^{ho}$	0.33
Crane move costs	$ct^{ho}$	0.5

Table 3: Environment parameters.

Settings		Projection Algorithms		Vanilla Algorithms	
Hyperparameters	Symbol	PPO	SAC	PPO	SAC
Actor Network		Attention	Attention	Attention	Attention
Number of Heads		8	8	4	4
Hidden Layer Size		128	128	256	256
Encoder Layers		3	3	2	1
Decoder Layers		3	3	3	3
Critic Network		$1 \times \text{MLP}$	$2 \times \text{MLP}$	$1 \times \text{MLP}$	$2 \times \text{MLP}$
Critic Layers		4	4	4	4
Target Network		No	Soft Update	No	Soft Update
Target Update Rate	$\tau$	N/A	0.005	N/A	0.005
Dropout Rate		0.009	0.009	0.073	0.164
Max Policy Std.		1.931	1.931	1.118	1.779
Optimizer		Adam	Adam	Adam	Adam
Learning Rate	$\eta$	$2.04 \times 10^{-4}$	$2.04 \times 10^{-4}$	$9.64 \times 10^{-4}$	$9.10 \times 10^{-4}$
Batch Size		64	64	64	64
Embedding Size		128	128	128	128
Discount Factor	$\gamma$	0.99	0.99	0.99	0.99
GAE	$\lambda$	0.95	N/A	0.95	N/A
Value Coefficient	$\lambda_c$	0.50	N/A	0.50	N/A
Entropy Coefficient	$\lambda_e$	0.010	Learned	0.061	Learned
Feasibility Penalty	$\lambda_f$	0.0677	0.0677	0.302	0.065
Clip Parameter	$\epsilon$	0.2	N/A	0.2	N/A
Replay Buffer		No	Yes	No	Yes
Replay Buffer Size		N/A	$10^4$	N/A	$10^4$
Mini-batch Size		16	16	32	16
Update Epochs		5	1	1	1
Entropy Target		N/A	$- X $	N/A	$- X $
Projection Learning Rate	$\eta_v$	0.05	0.05	N/A	N/A
Projection Epochs		100	100	N/A	N/A
Inference Projection Stop	$\delta_v$	100	100	N/A	N/A
Training Budget		$7.2 \times 10^7$	$7.2 \times 10^7$	$7.2 \times 10^7$	$7.2 \times 10^7$
Validation Budget		$5.0 \times 10^3$	$5.0 \times 10^3$	$5.0 \times 10^3$	$5.0 \times 10^3$
Validation Frequency		Every 20%	Every 20%	Every 20%	Every 20%

Table 4: Comparison of hyperparameters for projected and vanilla PPO and SAC.

Methods					Testing ( $N = 30$ )			
Alg.	Model	F.M.	H.P.	$\lambda_f$	Ob. (\$)	Time (s)	F.I. (%)	$d(PH(s_t))$
SAC	AM	FR	Proj.	0.0677	1139.78 <sup>†</sup>	13.82	0.00	62.77
SAC	AM	FR	Proj.	0.677	1031.55 <sup>†</sup>	13.45	0.00	120.74
SAC	AM	FR	Tune	0.065	1113.03 <sup>†</sup>	12.63	0.00	37.55
PPO	AM	FR	Proj.	0.0677	2606.87 <sup>†</sup>	13.36	0.00	3171.86
PPO	AM	FR	Proj.	0.677	2593.29 <sup>†</sup>	13.20	0.00	3381.59
PPO	AM	FR	Tune	0.302	1842.46 <sup>†</sup>	11.74	0.00	754.21

Table 5: Performance evaluation on  $N$  instances of feasibility regularization (FR) with hyperparameter (H.P.) settings: projected hyperparameters (Proj.), ensuring a fair comparison with projection-based policies, and tuned hyperparameter (Tune), optimized specifically for PPO and SAC with FR. While we use  $\lambda_f$  as the control parameter for FR, tuning involves adjusting a Lagrangian multiplier for each constraint. Average performance metrics include objective value in profit (Ob.), inference time in seconds (Time), percentage of feasible instances (F.I.), and total absolute distance to the feasible region  $d(PH(s_t))$ . Note that <sup>†</sup> indicates infeasible objectives.